AD-A097 363 CORNELL UNIV ITHACA N Y LAB OF ATOMIC AND SOLID STA--ETC F/G 7/4
AN EXPERIMENTAL STUDY OF ELECTRONIC STATES AT METAL-DIELECTRIC --ETC(U)
MAR 81 A J SIEVERS AFOSR-78-3684

UNCLASSIFIED AFOSR-TR-81-0334 NL

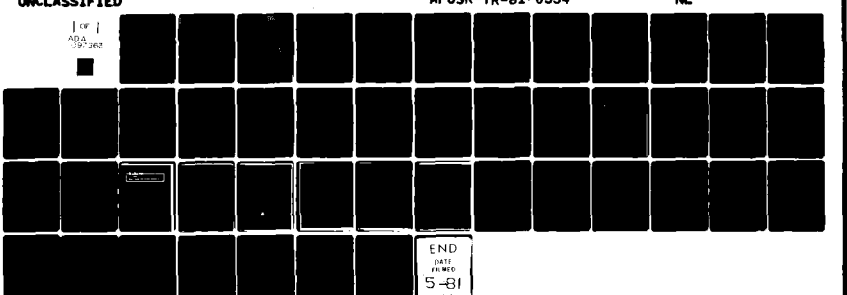

UNCLASSIFIED

SECURITY CLASSIFICATION OF THIS PAGE (When Data Entered)

REPORT DOCUMENTATION PAGE	READ INSTRUCTIONS BEFORE COMPLETING FORM
1. REPORT NUMBER: AFOSR-TR-81-0334	2. GOVT ACCESSION NO.: AD-A097363
3. RECIPIENT'S CATALOG NUMBER: 4	
4. TITLE (and Subtitle): AN EXPERIMENTAL STUDY OF ELECTRONIC STATES AT METAL-DIELECTRIC INTERFACES	5. TYPE OF REPORT & PERIOD COVERED: FINAL
	6. PERFORMING ORG. REPORT NUMBER
7. AUTHOR(s): A.J. Sievers, Professor of Physics	8. CONTRACT OR GRANT NUMBER(s): AFOSR-78-3684
9. PERFORMING ORGANIZATION NAME AND ADDRESS: Lab. of Atomic and Solid State Physics, Cornell University, Ithaca, NY 14853	10. PROGRAM ELEMENT, PROJECT, TASK AREA & WORK UNIT NUMBERS: 61102F 2306/B2
11. CONTROLLING OFFICE NAME AND ADDRESS: AFOSR/NE, Bolling AFB, DC 20332	12. REPORT DATE: 13 March 1981
	13. NUMBER OF PAGES: 43
14. MONITORING AGENCY NAME & ADDRESS (if different from Controlling Office)	15. SECURITY CLASS. (of this report): unclassified
	15a. DECLASSIFICATION/DOWNGRADING SCHEDULE

16. DISTRIBUTION STATEMENT (of this Report)

Approved for public release; distribution unlimited.

17. DISTRIBUTION STATEMENT (of the abstract entered in Block 20, if different from Report)

18. SUPPLEMENTARY NOTES

19. KEY WORDS (Continue on reverse side if necessary and identify by block number)

Spectroscopic techniques
Metal/Dielectric Interfaces

20. ABSTRACT (Continue on reverse side if necessary and identify by block number)

During the past 24 months we have succeeded in developing two new infrared techniques which are ideally matched for the spectroscopic investigation of metal dielectric interfaces. The first technique is surface wave interferometry, which is described in Reports A, B and D. We show that edges, steps or dielectric discontinuities on metal surfaces produce two kinds of propagating waves: surface plasmons which are bound to the surface and bulk electromagnetic radiation. Since both waves are coherent interfe-

DD FORM 1 JAN 73 1473

UNCLASSIFIED

AD A097363

20.

rence effects can be readily observed. A two beam interferometer has been constructed on the metal surface to demonstrate the interference phenomena and also to provide an interferometric wavelength measurement of infrared surface waves. The geometry appears well suited for heterodyne spectroscopic study of surface states.

The second technique is broad band surface electromagnetic wave spectroscopy, which is described in Reports C and E. The frequency range investigated so far is from 600 to 1800 cm^{-1}. A sharp absorption line near 1000 cm^{-1} in a molecular overlayer was used to compare the surface electromagnetic waves (SEW) and surface reflection spectroscopy techniques (SRS). The integrated optical density of the absorption line is an order of magnitude larger with SEW than with SRS, demonstrating conclusively that SEW is the more sensitive technique. We anticipate that the SEW broadband technique will be particularly useful for the spectroscopic investigation of the first steps of metal oxide growth.

LEVEL II

12

FINAL SCIENTIFIC REPORT

An Experimental Study of Electronic States at Metal-Dielectric Interfaces

Contract #AFOSR-78-3684

Submitted to: AFOSR/NE (Attn: J.P. Parsons)

Submitted by: Laboratory of Atomic and Solid State Physics
Cornell University
Ithaca, NY 14853

Principle Investigator: A.J. Sievers, Professor of Physics

STAFF: A.K. Chin
Z. Schlesinger
B. Webb
E.A. Schiff
T.R. Gosnell
L.H. Greene
R.P. Devaty

March 13, 1981

TABLE OF CONTENTS

March 13, 1981 Contract #AFOSR-78-3684

FINAL REPORT

An Experimental Study of Electronic States at Metal-Dielectric Interfaces

A.J. Sievers

Laboratory of Atomic and Solid State Physics
Cornell University
Ithaca, NY 14853

I. SUMMARY

During the past 24 months we have succeeded in developing two new infrared techniques which are ideally matched for the spectroscopic investigation of metal dielectric interfaces. The first technique is surface wave interferometry, which is described in Reports A, B and D. We show that edges, steps or dielectric discontinuities on metal surfaces produce two kinds of propagating waves: surface plasmons which are bound to the surface and bulk electromagnetic radiation. Since both waves are coherent interference effects can be readily observed. A two beam interferometer has been constructed on the metal surface to demonstrate the interference phenomena and also to provide an interferometric wavelength measurement of infrared surface waves. The geometry appears well suited for heterodyne spectroscopic study of surface states.

The second technique is broad band surface electromagnetic wave spectroscopy, which is described in Reports C and E. The frequency range investigated so far is from 600 to 1800 cm^{-1}. A sharp absorption line near 1000 cm^{-1} in a molecular overlayer was used to compare the surface electromagnetic waves (SEW) and surface reflection spectroscopy techniques (SRS). The integrated optical density of the absorption line is an order of magnitude larger with SEW than with SRS, demonstrating conclusively that SEW is the more sensitive technique. We anticipate that the SEW broadband technique will be particularly useful for the spectroscopic investigation of the first steps of metal oxide growth.

II. TECHNICAL ACCOMPLISHMENTS

(A) New Infrared Techniques

(1) Surface Wave Technique

We describe an interference phenomena which can occur on coated metal surfaces due to the tendency of a SEW to radiate two coherent beams when the nature of the surface supporting it changes. We demonstrate this effect with a two beam interferometer of variable path length in which the SEW's comprise one arm and the bulk waves the other. The observed interferograms and their Fourier transforms are in good agreement with model predictions.

Below the surface plasmon cutoff frequency the interface between the semi-infinite half spaces of metal supports a single bound TM mode. The SEW propagates along the interface and its field amplitudes decay exponentially with distance away from the interface.

There may be several such modes for a metal surface covered with a thick dielectric overlayer of thickness d. For a given infrared frequency the real and imaginary parts of the refractive index of these modes as a function of overlayer thickness are illustrated in Figure 1. In Figure 1b is shown the real part, which varies monotonically from just above the value for vacuum to approximately that of the dielectric overlayer itself while in Figure 1c is shown the absorption coefficient of the j^{th} mode. Also shown in the top of Figure 1 is the mode range, which characterizes the spatial extent of the intensity profile of the j^{th} mode above the metal surface. This precipitious change of the range in a region of overlayer thickness, where the index and the absorption coefficient are small, can produce a novel interference phenomena unique to inhomogeneous propagating waves.

To illustrate the interference phenomena, we consider a metal surface which is partially covered with a thick dielectric layer as illustrated in Figure 2a. the propagation of radiation across a step discontinuity in the overlayer thickness can be viewed in terms of the coupling of the normal modes on one side to the normal modes on the other.

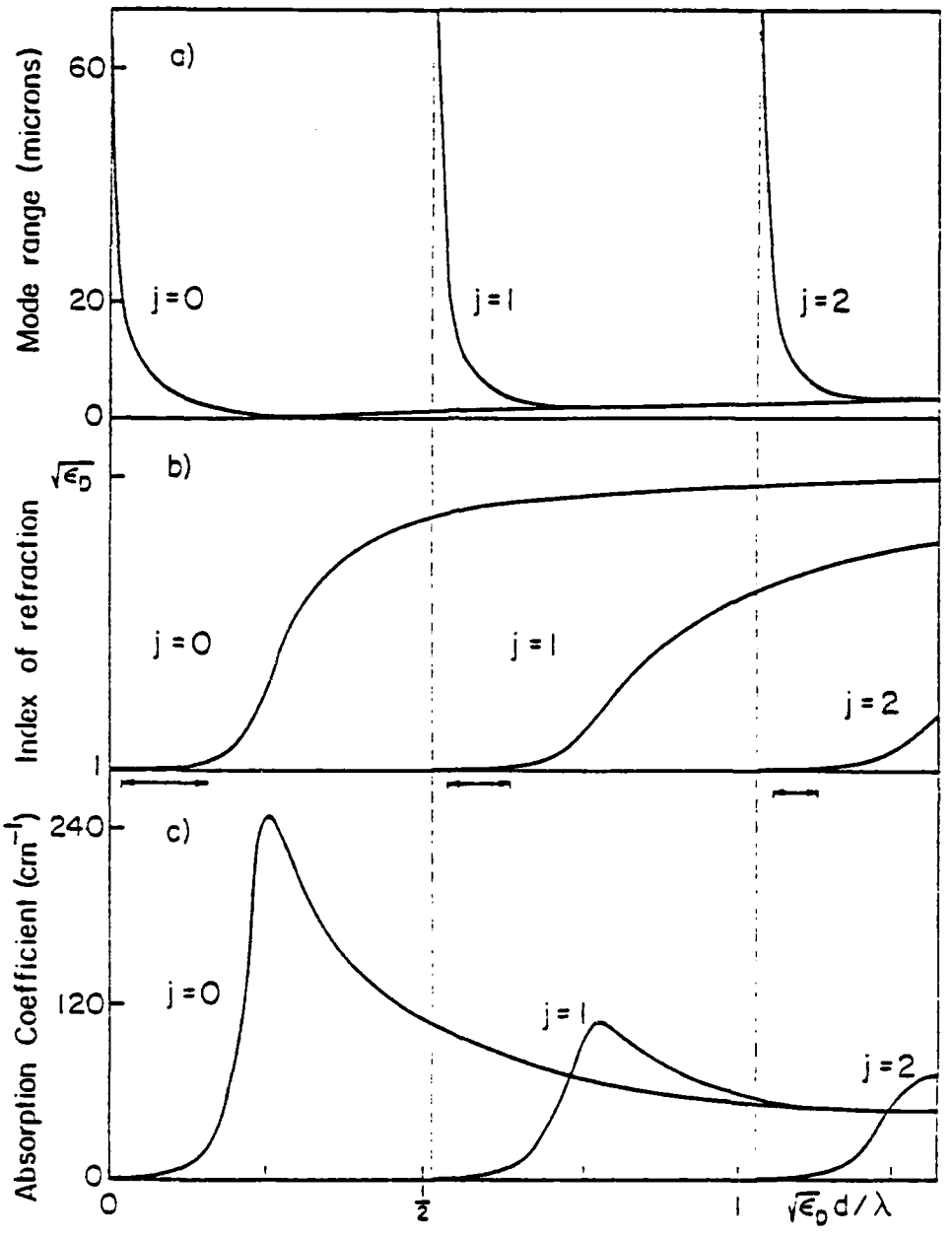

Figure 1 Optical constants of SEW modes for dielectric coated metal surfaces. a) the range: b) the effective index of refraction: and c) the absorption coefficient of the bound mode j are shown as a function of overlayer thickness d for a fixed infrared frequency, w. The horizontal arrows in (b) indicate the film thickness for which the interference effect should be large. The numerical values are for Ge coated Au at 10.6 micron wavelength.

In particular, consider a SEW on the bare metal, $z > 0$, travelling toward the step discontinuity in Figure 2. Since the discontinuity is small, reflection and refraction are small. One might expect the incident SEW to couple predominantly to the SEW of the coated region since both are bound modes; however, even for fairly thin overlayers the range of the SEW above the coated metal surface is much less than that of the SEW above the bare metal as shown in Figure 3. The boundary conditions (at $z = 0$) can be satisfied only if the incident SEW produces unbound bulk radiation in addition to the transmitted SEW.

This bulk radiation is produced in the form of a packet traveling in the - z direction and spreading slowly in the x direction. The SEW travels along the coated surface with a phase velocity c/n_o while the phase velocity of the bulk wave packet which travels above the overlayer is c. At the far edge of the overlayer, $z = \ell$, the SEW and the bulk wave packet both contribute to the transmission of a bare metal SEW, however these two contributions will in general no longer be in phase. The total intensity of the resultant SEW launched at $z = \ell$ can be written:

$$I(\ell) = I_{SEW}(\ell) - I_B(\ell) + 2\sqrt{I_{SEW}(\ell) \quad I_B(\ell)} \cos\left[\frac{\omega}{c}(n_o - 1)\ell\right] \quad (1)$$

where $I_{SEW}(\ell)$ and $I_B(\ell)$ are the component intensities. Because $n_c - 1$ is small, large interference periods will be produced by relatively short wavelength radiation (e.g. $\Delta\ell = 3$ mm at $\lambda = 10\ \mu$). To test these conclusions, evaporated Ag and Au films

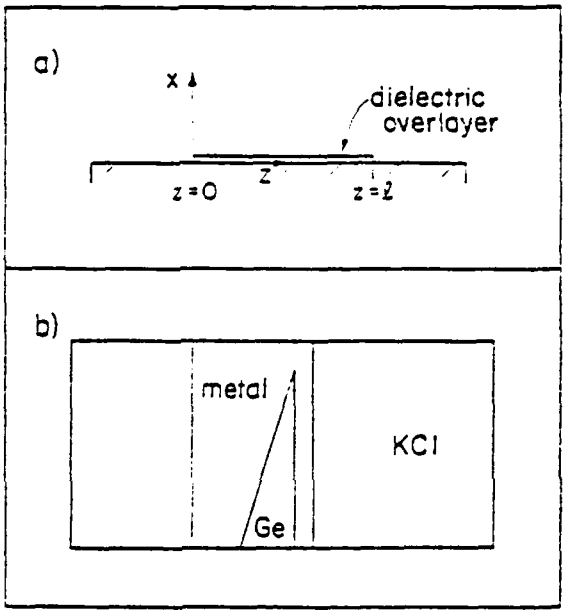

Figure 2. (a) Coordinate system for dielectric layer on a metal surface. (b) Top view of the surface wave interferometer. Both the metal and the Ge overlayer are evaporated onto the KCl coupler. The incident surface wave propagates from left to right. To change the Ge overlayer path length, the entire assembly is translated towards the top or bottom of the Figure. For the thin overlayer films described in the text both reflection and refraction of waves at the overlayer boundary can be ignored.

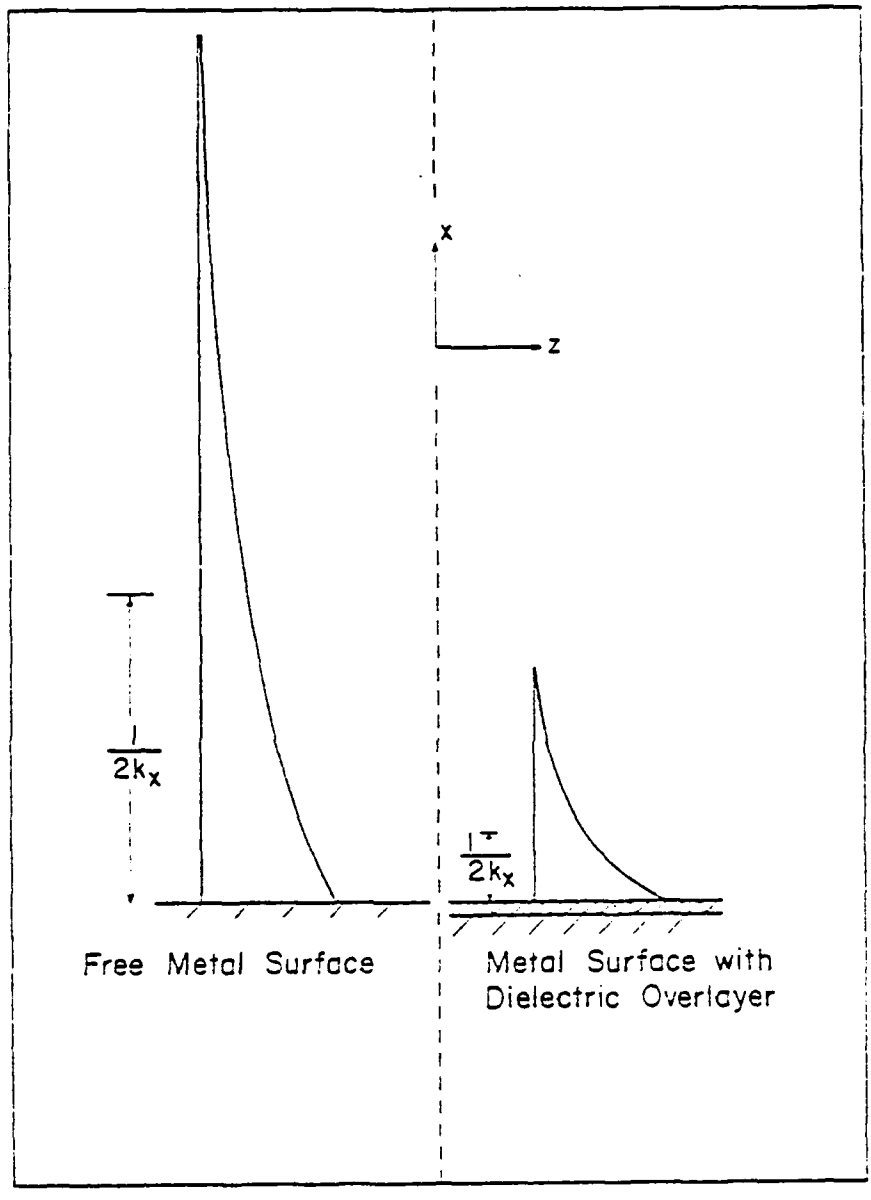

Figure 3. The range of the SEW above a coated and uncoated metal surface.

were deposited on KCl couplers. Over part of these rectangularly shaped films thin Ge overlayers of a triangular shape were then deposited, as shown in Figure 2b.

The SEW was launched from a CO_2 laser beam at one edge of the metal film by means of the edge coupling technique. At the corresponding point on the opposite edge of the metal the SEW produced at $z = \ell$ coupled into the dielectric and was detected. The length, ℓ, of the overlayer region probed by the beam was continuously varied by translating the film assembly in the plane of the surface but perpendicular to the beam direction.

An example of the observed transmission versus ℓ showing interference between a SEW and bulk radiation is presented in Figure 4. Another thickness film again showing interference is presented in Figure 5a along with the Fourier transform of the interferogram in Figure 5b.

The effect that leads to the SEW interferometer, namely the substantial coupling of the SEW to bulk radiation at discontinuities can be used to advantage for interface spectroscopy. The bulk radiation generated does not sample the metal dielectric interface whereas the SEW does; hence, an electric current at the interface only influences one beam of this double beam interferometer.

(2) Broad Band Surface Wave Spectroscopy

In previously reported work SEW's excited by coherent

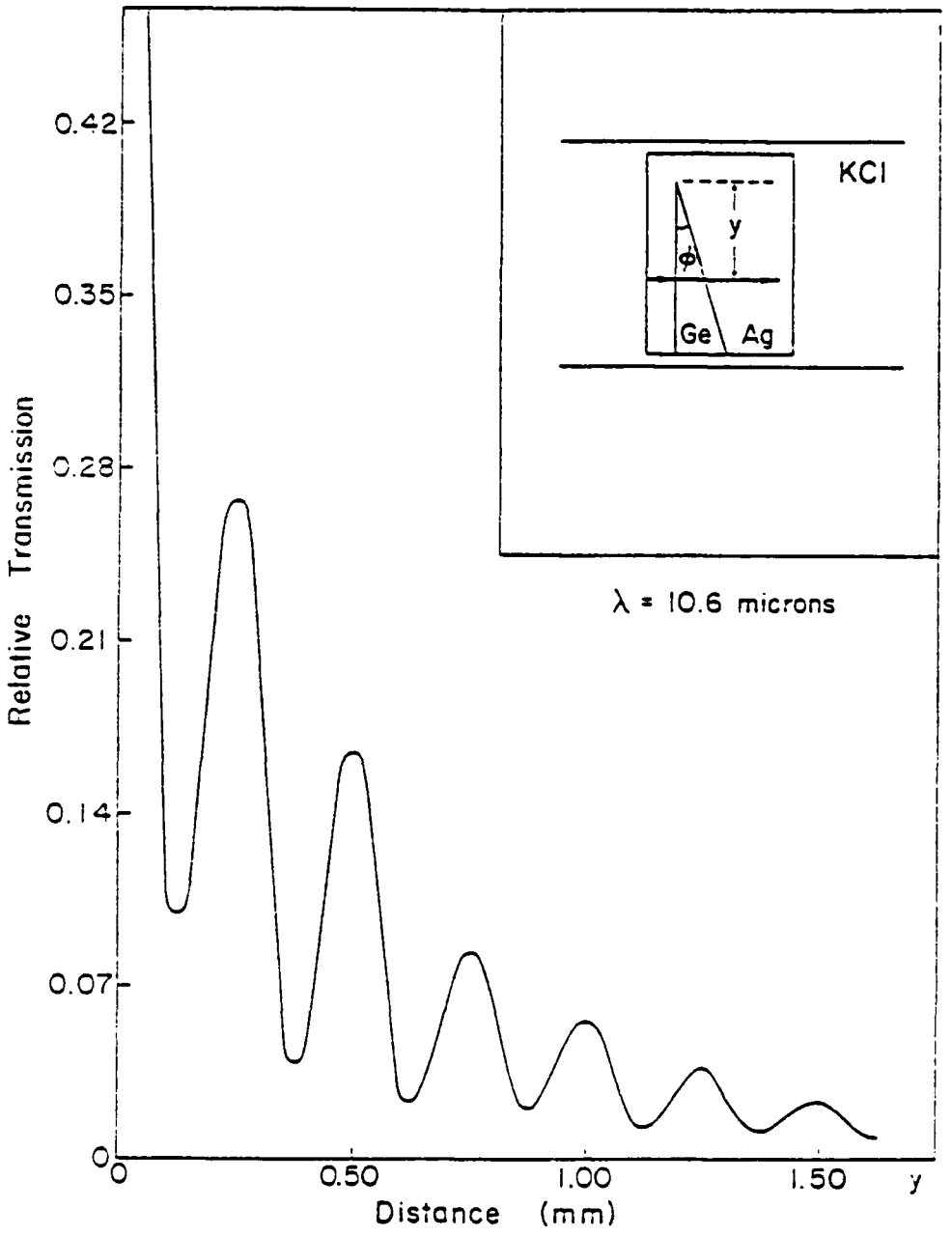

Figure 4. Optical path dependence of the relative transmission of an SEW across a dielectric film on a metal surface.

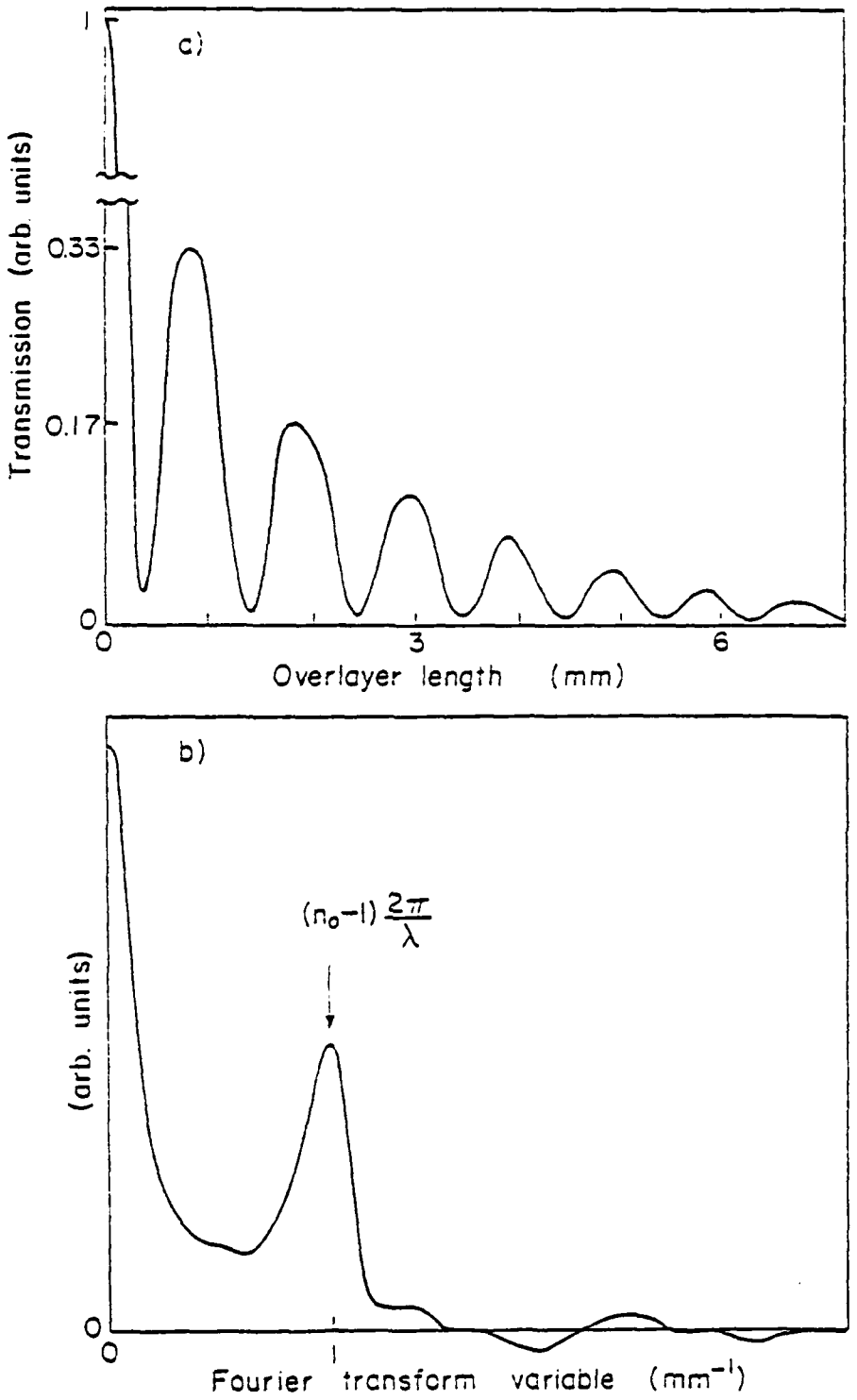

Figure 5. (a) Transmission of a Ge coated silver surface vs. optical path. The Ge coating is d = 0.2μ thick and the laser frequency is 975 cm^{-1}. (b) Fourier transform of the interferogram in (a).

radiation from infrared lasers have been propagated across metal and dielectric coated metals using the prism coupler shown in Figure 6a. This two prism coupling scheme first reported by Otto can be used to launch and recover monochromatic SEW's because the coupling efficiency is largest near the critical angle, θ_c, defined as

$$\theta_c = \sin^{-1}(n^{-1}) \qquad (2)$$

where n is the frequency dependent index of refraction of the prism. Since both the critical angle and the optimal gap spacing between the prism and the metal are frequency dependent then for a given alignment of the incident beam and the prism, efficient coupling can be achieved only for a narrow band of frequencies.

Our newly developed polychromatic coupling geometry is shown in Figure 6b. Transverse magnetic radiation (TM) polarized in the plane of the Figure 6b is incident on the coupler at a fixed angle θ_c (in the neighborhood of Brewster's angle). It enters the coupler at the frequency dependent angle

$$\theta_1 = \sin^{-1}(n^{-1}\theta_c) \quad . \qquad (3)$$

The beam is internally reflected off the metal film at point a and launches SEW's at the edge of the metal film at point b. The angle of incidence at the metal edge is

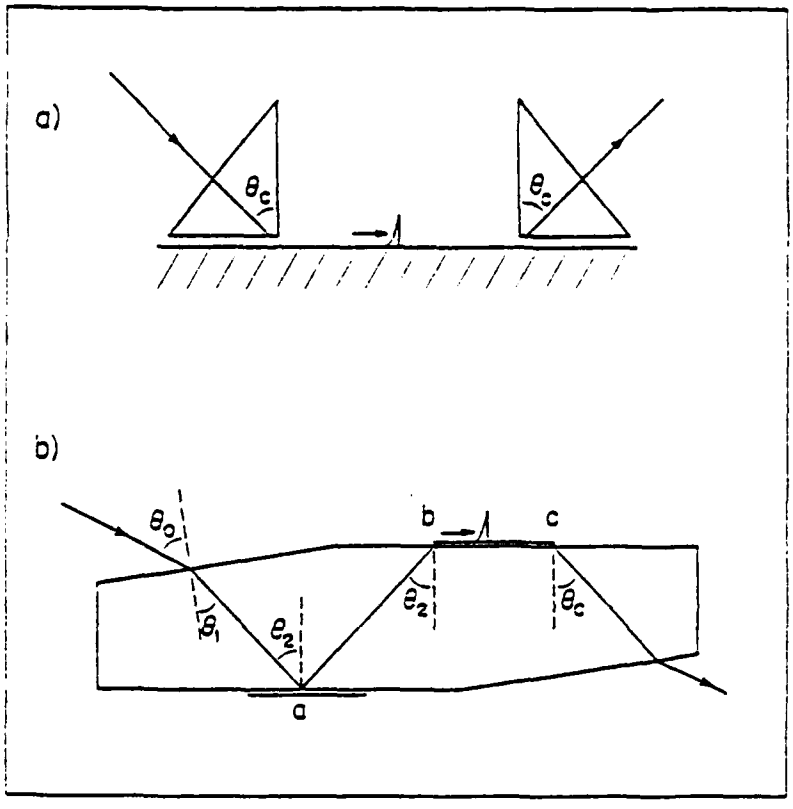

Figure 6a. The two prism evanescent wave coupler technique for launching and recovering monochromatic SEW's (After Otto).
Figure 6b. The edge coupler technique for launching and recovering polychromatic SEW's. The dispersive refraction of the incident beam partially compensates for the frequency dependence of the coupling angle. (The reflection at "a" causes the input and output beams to be parallel.)

$$\theta_2 = \gamma - \sin^{-1}\left[n^{-1}\sin\theta_c\right] \qquad (4)$$

where γ is the angle between the parallelepiped faces. A comparison of Equation 4 and Equation 2 shows that θ_2 and θ_c now depend similarly on frequency. If the edge coupler in Figure 6b is aligned for optical coupling at a particular frequency, then it will also necessarily be aligned for efficient coupling over a broad frequency region centered around that frequency.

To explore the sensitivity of the SEW technique, Au and Ag metal films were thermally evaporated at 2×10^{-6} torr background pressure. Next without breaking the vacuum a few monolayers of $KReO_4$ were evaporated over parts of the metal films. The polychromatic SEW measurement consisted of focusing a pencil of radiation from a Nernst glower source at the edge of the metal film to be studied. This beam, which is focused with parabolic mirrors, excites SEW's which traverse the surface and reappear at the far edge of the film as a collimated beam radiated into the coupler at the critical angle, θ_c. This slightly divergent beam is directed into a step and integrate Michelson interferometer and then focused on an As:Si photoconductive detector.

The spectrum of the SEW transmission across a 1.2 cm gold film is shown in Figure 7a. The low frequency cutoff at 700 cm^{-1} is due to bulk absorption in the KCl coupler. Increasing SEW attenuation and diminishing beam splitter and detector

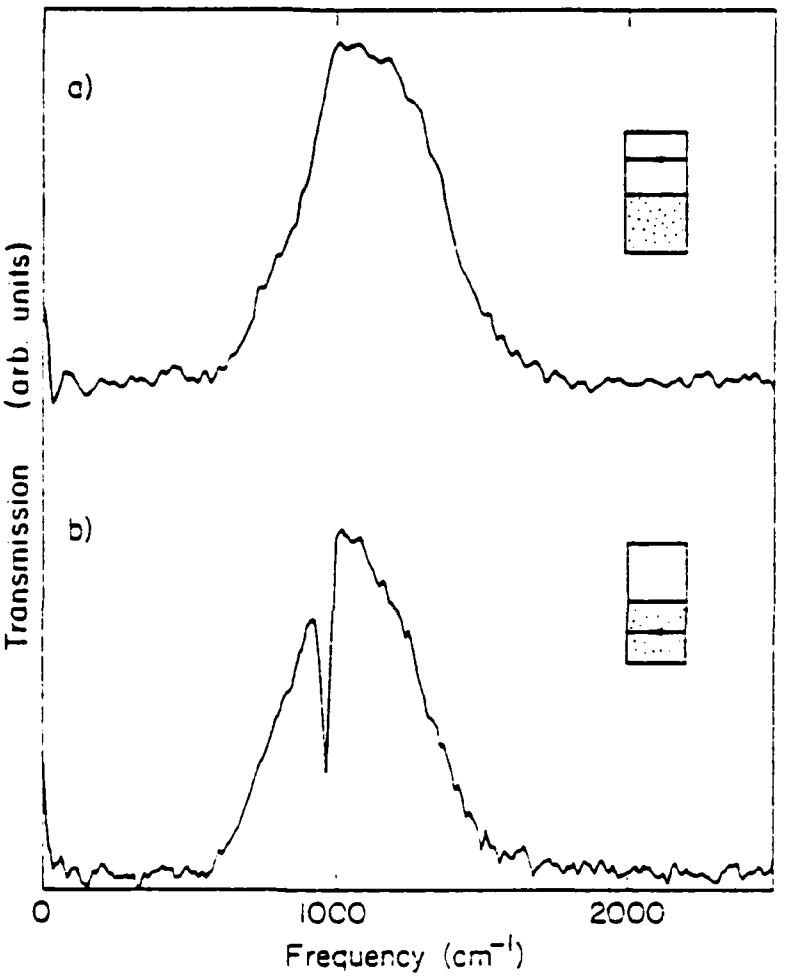

Figure 7a. The polychromatic spectrum of SEW's across a metal film. The low frequency cutoff at 700 cm^{-1} is due to bulk absorption in the KCl coupler. The 1.2 cm long Au film determines the high frequency cutoff at 1800 cm^{-1}.

Figure 7b. The same metal film covered with a few monolayers of $KReO_4$. The 20% deep absorption line at 930 cm^{-1} is due to the triply degenerate ν_3 mode of the ReO_4^- molecule.

efficiency all contribute to the 1800 cm^{-1} high frequency cutoff. In Figure 7b the spectrum of the $KReO_4$ covered region of the same gold film is shown. The 40% deep line at 930 cm^{-1} is due to the triply degenerate ν_3 mode of the ReO_4 molecule.

This is the first time that broadband generation and spectroscopic detection of infrared surface electromagnetic waves have been carried out. By replacing the KCl beam splitter and coupler with KRS-5 the lower frequency limit can be extended from 700 down to 200 cm^{-1}. By traversing shorter metal paths the high frequency region can be extended above 1800 cm^{-1}.

B. A New Metal-Semiconductor Composite Material

While our high vacuum multisource evaporator was being assembled, some exploratory infrared studies were made on a new class of semiconductor-metal two phase systems.

To grow a two phase semiconductor crystal, one starts with a eutectic mixture of InSb-NiSb headed above the melting point and then lowers it at constant velocity (e.g., 1 cm/hr) through a steep temperature gradient. Because of this crystal growing technique, the alloy is constrained to undergo a transformation unidirectionally with constant velocity. A transverse section normal to the growth axis reveals a periodic arrangement of NiSb rods (1 micron in diameter) in an InSb matrix. The periodic growth is controlled by diffusion. The more uniform the temperature gradient the more perfect the periodic arrays.

The d.c. electrical properties of the two phase InSb-NiSb

eutectic are to a large extent controlled by the parallel aligned metallic NiSb fibers within the semiconducting InSb matrix. Qualitatively, the combination of the two materials in this form results in a medium with highly anisotropic electrical properties. The electrical conductivity is large in the direction of the NiSb fibers and relatively small in the direction orthogonal to the fibers. Also, due to the NiSb fibers, this eutectic displays magneto-resistive properties even more dramatic than those of pure InSb. Although the energy band structure of this material has not yet been determined, a number of practical devices have already appeared.

In our investigation a series of infrared measurements have been made when temperature, sample orientation and magnetic field are systematically vaired (Report F). For the most part the properties of the eutectic have been found to be similar but not identical to those of P-type InSb.

One interesting effect which is associated directly with the NiSb rods is a shape resonance in the far infrared spectral region. Electromagnetic radiation can excite the odd harmonics of the longitudinal surface plasmon modes of these rods which are about 1 micron in diameter and 20 microns long. For the particular eutectic studied the lowest mode is at 60 cm^{-1}, the next is at 180 cm^{-1} and the third is at 300 cm^{-1}. A detailed study of these resonances for both current and noncurrent carrying configurations should enable us to identify spectral features associated with non-equilibrium properties.

REPORTS AND PUBLICATIONS

A. "Surface Wave Interferometer for the Infrared Region", Z. Schlesinger, A.J. Sievers, and R. Warner, Opt. Soc. Am. 69, 1434 (1979).

B. "Surface Wave Interferometry", Z. Schlesinger and A.J. Sievers, Appl. Phys. Lett. 36, 409 (1980).

C. "Broad-Band Surface Electromagnetic Wave Propagation on Metal Surfaces", Z. Schlesinger, Y.J. Chabal and A.J. Sievers, Bull. Am. Phys. Soc. 25, 425 (1980).

D. "Interferometric Wavelength Measurement of Infrared Surface Waves", Z. Schlesinger and A.J. Sievers, Basic Optical Properties of Materials, A. Feldman, ed. (National Bureau of Standards Pub. 574, 1980), p. 238.

E. "Broad Band Surface Electromagnetic Wave Spectroscopy", Z. Schlesinger and A.J. Sievers, Surface Science Letters 102, L29 (1981).

F. "Intraband Magneto-Optical Studies of InSb-NiSb Eutectic", A.K. Chin and A.J. Sievers, Journal of Magnetism and Magnetic Materials 11, 109 (1979).

G. "Origins of Very Shallow Photoconduction in Ge:Sb", E.A. Schiff, Solid State Commun. 35, 991 (1980).

JOURNAL
of the
OPTICAL SOCIETY
of
AMERICA

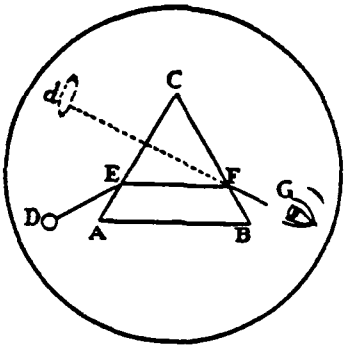

OCTOBER

1979

VOLUME 69 NUMBER 10

STANLEY J. REFERMAT, *Presider*

Thin Film Characterization

Contributed Papers

WH1. Automatic High-Precision Determination of the Optical Thickness of Thin Films. L. M. SMITHLINE AND G. J. WOLGA, *Lansing Research Corporation, P. O. Box 730, Ithaca, NY 14850.*—A new instrument has been designed, constructed, and operated for the purpose of determining the optical thickness of homogeneous transparent single-optical films on plane substrates. Optical thickness is measured by determining the wave number of reflected or transmitted light such that the reflection or transmission is an extremum together with the order of interference. The device is capable of "locking on" to an extremum of either sense automatically and interpreting the lock condition in terms of optical thickness. Optical thickness is determined with a precision of better than 1 Å, and the spectral calibration of the instrument is accurate to better than ±2 cm^{-1}. The instrument is capable of performing the control/monitor function during thin film deposition and can be designed to operate in the near infrared as well as in the visible. The instrument's performance will be illustrated by data obtained from measurements on MgF_2 films on glass and sapphire films on silicon. (13 min.)

WH2. New Method for Determining the Optical Parameters of Fluorescent or Scattering Thin Films. W. LUKOSZ AND R. E. KUNZ, *Swiss Federal Institute of Technology, ETH, 8093 Zürich, Switzerland.*—We have determined the refractive index n_0 and the thickness d_0 of fluorescing thin films by comparing measured and calculated angular intensity distributions of the s- and p-polarized fluorescent light originating in the film. For evaporated layers of europium-chelate EuBTF we obtained $n_0 = 1.57$ at $\lambda = 612$ nm, and, *e.g.*, $d_0 = 30$ nm. We found the fluorescence at this wavelength to be emitted in electric-dipole transitions, the dipole moments being randomly oriented. The method is based on our calculation of the radiation patterns of electric and magnetic dipoles with arbitrary orientation embedded in the film (*o*) which is assumed to be sandwiched between two dielectric media of refractive indices n_1 and n_2, respectively. Generalizing results for dipoles close to a single dielectric interface,[1] we have solved the electromagnetic boundary value problem rigorously. The potential and the limitations of the method will be discussed, also the use of Raman or Rayleigh scattering in the film instead of its fluorescence. (13 min.)

[1] W. Lukosz, "Light emission by electric and magnetic dipoles close to a dielectric interface," J. Opt. Soc. Am. 68, 1406 (1978).

WH3. Surface-Wave Interferometer for the Infrared Region.* Z. SCHLESINGER, A. J. SIEVERS, AND R. WARNER, *L.A.S.S.P., Cornell University, Ithaca, NY 14853.*—We have studied the transmission of 9.2 to 10.8 μm wavelength surface waves across Au and Ag films which are partially covered by thin Ge overlayers. Although the overlayer thickness d is much less than the wavelength ($d/\lambda < 0.05$), strong periodic oscillations are observed in the transmission as a function of the overlayer thickness d, the overlayer length l, and the wavelength λ. The oscillations are produced by interference between a surface wave and a bulk wave both of which are coherently launched at one edge of the Ge overlayer and then recombined to interfere constructively or destructively at the other edge. Using this beam-splitting property of the overlayer edge, a new type of surface-wave interferometer has been constructed in which l is varied continuously. From the experimental interferogram the effective index of refraction and absorption coefficient of the overlayer—metal systems are obtained simultaneously. This technique measures n with about 100 times the precision of previously used techniques such as attenuated total reflection. (13 min.)

* Supported by Air Force Office of Scientific Research Contract No. AFOSR-78-3684.

WH4. Color Variations of AR Coatings Caused by a Leached Substrate Layer. K. H. GUENTHER, *Thin Film Development Dept., Balzers AG, Balzers, Fuerstentum, FL9496 Liechtenstein.*—Color differences of AR-coated prisms were found to be due to a surface layer with a refractive index of $n = 1.46$ and a geometrical thickness of approximately 41 nm on the glass substrate (BaK_4, $n = 1.5688$). The existence of such a layer is demonstrated by reflection spectroscopy measurements which are in reasonable agreement with numerical calculations of the spectral reflectance of both the uncoated substrate and the coated one. An AES depth profiling analysis reveals the layer to consist of pure silica (SiO_2), the Ba content having been leached out completely. The reason for the formation of this leached substrate layer was an improper cleaning treatment of the uncoated prisms in the optical shop. (13 min.)

WH5. Microdensitometry Using Backscattered Electrons.* H. W. DECKMAN AND D. BLACK,† *Exxon Research and Engineering Company, P.O. Box 8, Linden, NJ 07036.*—We have demonstrated that the optical density of film (Kodak HRP) exposed with soft x rays can be measured using an electron beam rather than light to interrogate the emulsion layer. For soft-x-ray exposures, developed grains are located near the surface of the film and the fraction of electrons backscattered from silver in the emulsion layer is an accurate measure of optical density. Films have been imaged by collecting the backscattered electron fraction in both scanning and transmission electron microscopes with beam voltages of 25 and 40 kV, respectively. Changing incident beam voltage affects depth of electron penetration into the emulsion and thus the information content of the backscattered signal. Lateral spatial resolution of this imaging technique is determined by the intensity distribution of backscattered electrons emerging at the film surface and is estimated to be better than 0.5 μm. To correlate optical density with the backscattered electron fraction, a step-wedge exposure was prepared using a bremsstrahlung x-ray source obtained from a W target operated so that the cutoff in the spectrum was 3 Å. Specular density of the step-wedge exposure was measured with a Joyce Loebel densitometer and compared with the fraction of electrons backscattered from each region of the wedge. Results of these experiments indicate that microdensitiometry using backscattered electrons is a promising technique for examining film exposed with soft x rays. (13 min.)

* This work was partially supported by Exxon Research and Engineering Company, General Electric Company, Northeast Utilities, Empire State Electric Energy Research Corporation, and New York State Energy Research and Development Administration.

† Eastman Kodak Company.

WH6. Normal Incidence Soft-X-Ray Reflectors for Arbitrary Wavelengths Using a Modified Langmuir-Blodgett Method. ALAN E. ROSENBLUTH AND J. M. FORSYTH, *Institute of Optics and Laboratory for Laser Energetics, University of Rochester, Rochester, NY 14627.*—X-ray reflectors operating near normal incidence must contain a large number of (near) quarter-wave periods due to the weak interaction of x rays with matter. As a result, the production of such reflectors using conventional layer deposition techniques presents a challenging problem.[1] For wavelengths in the 100 Å regime, the stringent tolerances involved can be met using the Langmuir-Blodgett technique, in which successive portions of a monomolecular fatty-acid film are transferred from an aqueous to a solid substrate.[2] The technique may be modified in an effort to produce mirrors tuned to reflect arbitrary source wavelengths. One such modification makes use of mirrors in which different layers are formed from different

Infrared surface wave interferometry

Z. Schlesinger and A. J. Sievers
Laboratory of Atomic and Solid State Physics and Materials Science Center, Cornell University, Ithaca, New York 14853

(Received 21 November 1979; accepted for publication 7 January 1980)

An interference phenomena is described which involves infrared surface electromagnetic waves on coated metals. The interference is demonstrated with a two-beam surface wave interferometer of variable path length which utilizes the strong coupling between surface and bulk electromagnetic waves at coating edges.

PACS numbers: 42.10.Jd, 07.60.Ly

Infrared surface electromagnetic waves (SEW's) on metal surfaces have an inherent high sensitivity to surface coatings.[1-3] A variety of infrared (IR) SEW transmission studies have been reported in the literature.[2-8] In this letter we describe an interference phenomena which can occur on coated metal surfaces owing to the tendency of a SEW to radiate when the nature of the surface supporting it changes. We demonstrate this effect with a two-beam interferometer of variable path length in which the SEW's comprise one arm and the bulk waves the other. The observed interferograms and their Fourier transforms are in good agreement with model predictions.

Below the surface plasmon cutoff frequency $\omega_p/(1+\epsilon_D)^{1/2}$ the interface between the semi-infinite half spaces of metal (plasma frequency ω_p) and dielectric (dielectric constant ϵ_D) supports a single bound TM mode. The dispersion relation for this SEW mode is[9]

$$-\tilde{\epsilon}_m/\tilde{\delta} = \epsilon_D/\tilde{\beta}\,, \tag{1}$$

 0003-6951/80/060409-04$00.50

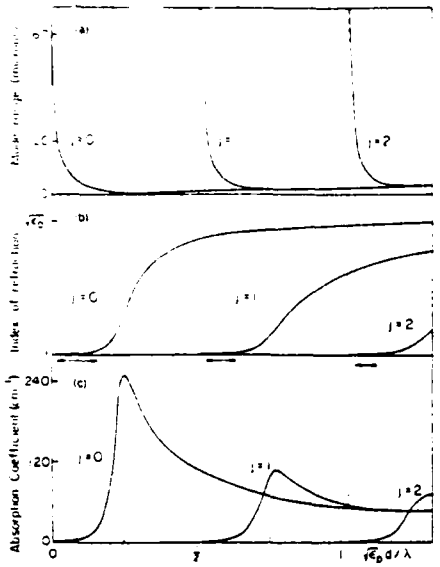

FIG. 1. Optical constants of SEW modes for dielectric coated metal surfaces: (a) range r_j, (b) effective index of refraction n_j, and (c) absorption coefficient α_j of the bound mode j are shown as a function of overlayer thickness d for a fixed IR frequency ω. The wavelength of a given mode is $\lambda_j = \lambda/n_j$, where λ is the free-space wavelength. The horizontal arrows in (b) indicate the fi'm thickness for which the interference effect should be large. The numerical values are for Ge-coated Au at a 10.6-μ wavelength.

where $\tilde{\epsilon}_m$ is the complex frequency-dependent dielectric function of the metal,

$$\tilde{\delta} = [\tilde{k}_{\parallel}^2 - (\omega^2/c^2)\epsilon_m]^{1/2} \tag{2}$$

and

$$\tilde{\beta} = [\tilde{k}_{\parallel}^2 - (\omega^2/c^2)\epsilon_D]^{1/2} . \tag{3}$$

In Eq. (2) and (3), $\tilde{k}_{\parallel}$ is the component of the complex propagation vector parallel to the interface. ω is the SEW frequency, and c is the speed of light. The SEW propagates along the interface and its field amplitudes decay exponentially with distance away from the interface with decay constants $\mathrm{Re}\tilde{\delta}$ in the metal and $\mathrm{Re}\tilde{\beta}$ in the dielectric.

There may be several such modes for a metal surface covered with a dielectric overlayer of thickness d whose dispersion relations may be obtained from the eigenvalue equation[10]

$$\tanh(\tilde{\beta}d) = -\epsilon_D\tilde{\beta}(\tilde{\epsilon}_m\tilde{\gamma} + \tilde{\delta})/(\tilde{\epsilon}_m\tilde{\beta}^2 + \epsilon_D\tilde{\gamma}\tilde{\delta}) , \tag{4}$$

where $\tilde{\gamma} = [\tilde{k}_{\parallel}^2 - (\omega^2/c^2)]^{1/2}$ and the $\tilde{\beta}$ and $\tilde{\delta}$ are again defined by Eq. (2) and (3). For a given IR frequency and overlayer thickness d, Eq. (4) has $M+1$ discrete solutions where M is the largest integer less than $2(\epsilon_D)^{1/2}d/\lambda$ and λ is the free-space wavelength. Each of these solutions corresponds to a bound mode of the metal-overlayer-air configuration. A given mode is characterized by its complex refractive index:

$$N_j = (c/\omega)\tilde{k}_j , \tag{5}$$

where $0 \leqslant j \leqslant M$. For a given IR frequency the real and imaginary parts of the refractive index of these modes as a function of overlayer thickness are illustrated in Fig. 1. In Fig. 1(b) is shown the real part $n_j = \mathrm{Re}(\tilde{N})$, which varies monotonically from just above the value for vacuum to approximately that of the dielectric overlayer itself, while in Fig. 1(c) is shown the absorption coefficient of the jth mode.

$$\alpha_j = (4\pi/\lambda)\mathrm{Im}(\tilde{N}_j) ,$$

which is sharply peaked at $(\epsilon_D)^{1/2}d/\lambda = \frac{1}{4}(2j-1)$.

Also shown in the top of Fig. 1 is the mode range r_j, which characterizes the spatial extent of the intensity profile of the jth mode above the metal surface. This quantity, defined in terms of the first moment of the intensity profile, is

$$r_j = \int_0^\infty x\frac{H_j^2(x)}{\epsilon(x)}dx \Big/ \int_0^\infty \frac{H_j^2(x)}{\epsilon(x)}dx , \tag{6}$$

where the metal occupies the half space $x<0$ and the vacuum $x>d$ and where $\epsilon(x)$ is a step function which takes the values of the dielectric constants in each medium. The inverse range r_j^{-1} can be interpreted physically as a measure of the boundness of the jth mode. At each mode turn on $[(\epsilon_D)^{1/2}d/\lambda = \frac{1}{4}j]$ r_j is quite large, as shown in Fig. 1(a), but it decreases rapidly with increasing d to a value on the order of the overlayer thickness d. This precipitous change of r_j in a region of overlayer thickness where $n_j - 1$ and α_j are small, can produce a novel interference phenomena unique to inhomogeneous propagating waves.

To illustrate the interference phenomena, we consider a metal surface which is partially covered with a thin dielectric overlayer $[(\epsilon_D)^{1/2}d/\lambda < \frac{1}{4}]$, as illustrated in Fig. 2(a). For a given IR frequency, both the normal electromagnetic modes of the metal-vacuum region at $z<0$ and the metal-overlayer-air region at $l \geqslant z \geqslant 0$ consist of one bound mode and a continuum of bulk modes. The propagation of radiation across a step discontinuity in the overlayer thickness can be viewed in terms of the coupling of the normal modes on one side to the normal modes on the other.

In particular, consider a SEW on the bare metal, $z<0$, traveling toward the step discontinuity in Fig. 2. Since the discontinuity is small, reflection and refraction are small.

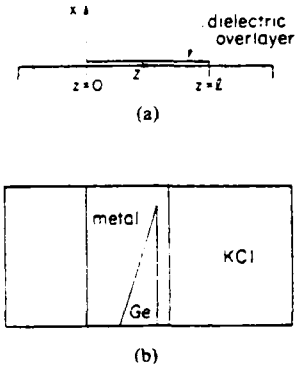

FIG. 2. (a) Coordinate system for dielectric layer on a metal surface. (b) Top view of the surface wave interferometer. Both the metal and the Ge overlayer are evaporated onto the KCl coupler. The incident surface wave propagates from left to right. To change the Ge overlayer path length, the entire assembly is translated towards the top or bottom of the figure. For the thin overlayer films described in the text both reflection and refraction of waves at the overlayer boundary can be ignored.

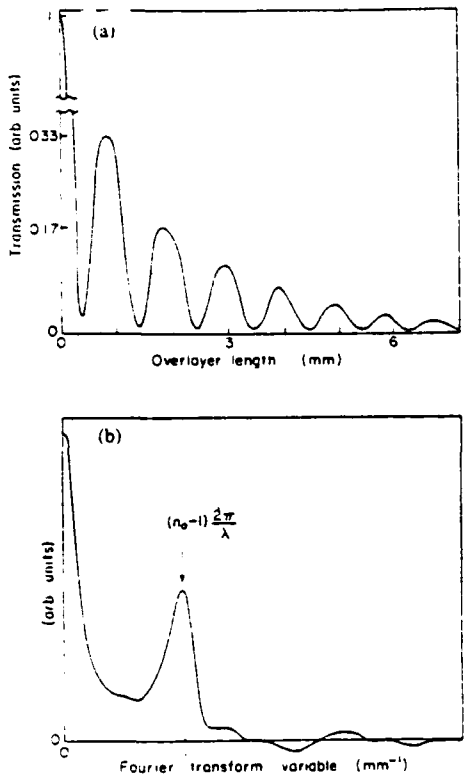

FIG. 3. (a) Transmission of a Ge-coated silver film vs optical path. The Ge coating is $d = 0.2\,\mu$ thick and the laser frequency is 975 cm^{-1}. (b) Fourier transform of the interferogram in (a).

One might expect the incident SEW to couple predominantly to the SEW of the coated region since both are bound modes; however, Maxwell's equations require that the tangential E and H fields be continuous across $z = 0$ at all heights x above the surface. Even for fairly thin overlayers $[(\epsilon_D)^{1/2}d/\lambda \gtrsim 0.005]$ the range of the SEW above the coated metal surface is much less than that of the SEW above the bare metal. The boundary conditions (at $z = 0$) can be satisfied only if the incident SEW produces unbound bulk radiation in addition to the transmitted SEW. For thicker overlayers $[(\epsilon_D)^{1/2}d/\lambda > \frac{1}{8}]$ the coated-metal SEW is so compressed that the incident bare-metal SEW cannot couple to it and almost all of the incident intensity is converted to bulk radiation. For thicknesses such that $0.005 \leqslant (\epsilon_D)^{1/2}d/\lambda \leqslant \frac{1}{8}$, the incident SEW launches both bulk and SEW radiation. This bulk radiation is produced in the form of a packet traveling in the $+z$ direction and spreading slowly in the x direction.[11] The SEW travels along the coated surface with a phase velocity c/n_0, while the phase velocity of the bulk wave packet which travels above the overlayer is c. At the far edge of the overlayer, $z = l$, the SEW and bulk wave packet both contribute to the transmission of a bare-metal SEW, however, these two contributions will in general no longer be in phase. The total intensity of the resultant SEW launched at $z = l$ can be written

$$I(l) = I_{\mathrm{SEW}}(l) + I_B(l) + 2\,[I_{\mathrm{SEW}}(l)I_B(l)]^{1/2}\cos[(\omega/c)(n_0-1)l\,]\,, \qquad (7)$$

where $I_{\mathrm{SEW}}(l)$ and $I_B(l)$ are the component intensities.[12] A bulk wave packet is also launched at $z = l$ with an interference term complementary to that of the $z > l$ SEW. The first two terms in Eq. (7) decrease monotonically with increasing overlayer length l:

$$I_{\mathrm{SEW}}(l) \propto e^{-\alpha l}, \quad I_B(l) \propto 1/l\,.$$

From the third term in Eq. (7), the spatial period of the interference is

$$\Delta l = \lambda/(n_0 - 1)\,. \qquad (8)$$

Because $n_0 - 1$ is small, large interference periods will be produced by relatively short-wavelength radiation (e.g., $\Delta l = 3$ mm at $\lambda = 10\,\mu$).

To test these conclusions, evaporated Ag and Au films were deposited on KCl couplers.[13] Over part of these rectangularly shaped films thin Ge overlayers of a triangular shape were then deposited, as shown in Fig. 2(b). Both the metal and Ge film evaporations were carried out at a pressure of 4×10^{-6} torr. The vacuum was not broken between evaporations.

The SEW was launched from a CO_2 laser beam at one edge of the metal film by means of the edge coupling technique.[14] At the corresponding point on the opposite edge of the metal the SEW produced at $z = l$ coupled into the dielectric and was detected. The length l of the overlayer region probed by the beam was continuously varied by translating the film assembly in the plane of the surface but perpendicular to the beam direction. The transmission was measured as a function of l for fixed overlayer thicknesses d and CO_2 laser frequency ω.

An example of the observed transmission vs l showing interference between a $j = 0$ SEW and bulk radiation is presented in Fig. 3(a) along with the Fourier transform of the interferogram in Fig. 3(b). Values of the interference period Δl are obtained either from the separation of the local maxima of the interferogram [Fig. 3(a)] or from the position of the peak in its Fourier transform [Fig. 3(b)]. Figure 4 shows

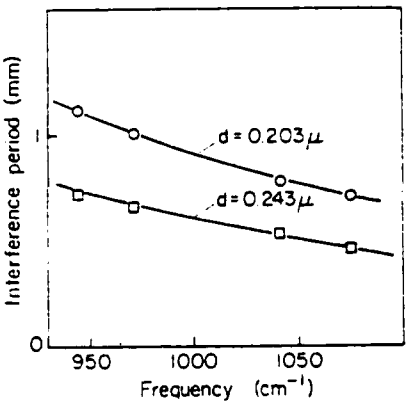

FIG. 4. Spatial period of interference vs laser frequency. The circles and triangles are the measured values of the interference period Δl for two different samples. The solid lines are calculated values of Δl for overlayer thicknesses 0.203 and 0.243, respectively.

a fit of $\Delta l(\omega;d)$ to the observed Δl for two films at four different frequencies using d as an adjustable parameter for each film. The period $\Delta l(\omega;d)$ is obtained from Eq. (8) with $n_{\parallel}(\omega;d)$ obtained from Eq. (4) using $\epsilon_D = 16$ and a Drude model[15] for $\tilde{\epsilon}_m$. The values of the Ge overlayer thickness thus obtained agree with measurements of the mechanical thickness as measured with a diamond stylus.[16]

In conclusion, we have described and demonstrated interference between the $j = 0$ SEW and bulk radiation. Interference between the next few higher-order SEW's and bulk waves can occur in a similar manner. The effect that leads to the SEW interferometer, namely, the substantial coupling of the inhomogeneous (bound) SEW to homogeneous (unbound) radiation can occur whenever the nature of the interface supporting a weakly bound SEW changes.

The authors wish to acknowledge useful conversations with R. Warner, Y. Chabal, and R.H. Silsbee. This work was supported by AFOSR under Grant No. AFSOR-76-3684. Additional support was received from the National Science Foundation under Grant No. DMR-76-81083 A02 to the Cornell Materials Science Center. This is Materials Science Center Report No. 4177.

[1]V. M. Agranovich, Sov. Phys. Usp. **18**, 99 (1975).
[2]K. Bhasin, D. Bryan, R.W. Alexander, and R.J. Bell, J. Chem. Phys. **64**, 5019 (1976).
[3]Y. J. Chabal and A.J. Sievers, J. Vac. Sci. Technol. **15**, 638 (1978).
[4]J. Schoenwald, E. Burstein, and J.M. Elson, Solid State Commun. **12**, 185 (1973).
[5]J.D. McMullen, Solid State Commun. **17**, 331 (1975).
[6]D.A. Bryan, D.L. Begley, K. Bhasin, R.W. Alexander, R.J. Bell, and R. Gerson, Surf. Sci. **57**, 53 (1976).
[7]D.L. Begley, D.A. Bryan, R.W. Alexander, R.J. Bell, and C.A. Goben, Surf. Sci. **60**, 99 (1976).
[8]D.L. Begley, R.W. Alexander, C.A. Ward, R. Miller, and R.J. Bell, Surf. Sci. **81**, 245 (1979).
[9]A. Otto, Z. Phys. **216**, 398 (1968).
[10]D. Marcuse, *Theory of Dielectric Optical Waveguides* (Academic, New York, 1974), p. 14.
[11]Calculations by the authors (unpublished).
[12]J.B. Marion, *Classical Electromagnetic Radiation* (Academic, New York, 1965), p. 336.
[13]Y. Chabal and A.J. Sievers, Appl. Phys. Lett. **32**, 90 (1978).
[14]The two-prism coupler used in Refs. 4–8 cannot discriminate between the SEW and low-lying bulk radiation, so no interference will be observed with this coupling geometry.
[15]H.E. Bennett and J.M. Bennett, in *Optical Properties and Electronic Structure of Metals and Alloys*, edited by F. Abeles (Wiley, New York, 1966), p. 175.
[16]The low precision of the stylus measurement does not permit us to extract the precise value of $(\epsilon_D)^{1/2}$ for the evaporated film.

Bulletin
of the
American Physical Society

Volume 25, Number 3, March 1980

PROGRAM OF THE 1980 MARCH MEETING IN NEW YORK, N.Y., 24–28 MARCH 1980

Published for the American Physical Society
by the American Institute of Physics

self-consistent vector potential which is used in the photon-electron transition matrix elements. Calculations are done for the frequency dependence of the magnitude of the cross section. Typical cross sections are of the order of $10^{-27}cm^2$ for the frequency of the incoming light in the vicinity of one-half the plasma frequency. This is still somewhat smaller than the experimentally observed cross section and it is believed that additional enhancement arises when the metal surface is rough.

*Supported by USDOE-contract No. AK-01-02-02-3.

NC 11 Surface Enhanced Raman Scattering: Angle Resolved Scattering and Substrate Dependence. T.E. FURTAK, G.R. TROTT, and B.H. LOO, Ames Lab.-USDOE* and Dept. of Physics., Iowa State Univ., Ames, IA 50011—The effects of independent variation of the incident angle, collection angle, and polarization of the incident and scattered radiation on the intensity of the Raman effect from cyanide adsorbed on silver are reported. The dependence of the anomalous enhancement on the nature of the substrate has also been investigated. Results are discussed for cyanide on alloys of silver with palladium, on copper, and on gold. These data are evaluated in terms of the role of surface plasmons and damping in the metal.

*Supported by USDOE-contract No. AK-01-02-02- .

NC 12 Enhanced Raman Scattering In Multi-layer Film Structures. D. L. ALLARA, M. RHINEWINE, C. A. MURRAY, Bell Laboratories. We have studied surface enhanced Raman scattering from organic molecules incorporated into structures consisting of two basic geometries:

1. CaF_2/Al (oxide covered)/organic scatterer/organic spacer/Ag; (reference 1)
2. Al (oxide covered)/organic scatterer/organic spacer /CaF_2/Ag

We study the Raman intensity both as a function of scatterer and spacer thickness, calibrated with IR absorption and ellipsometry. When no spacers are present we find samples of type 2 give comparable enhancements in cross section ($\sim 10^4$) to those of type 1, indicating that actual contact with Ag is unnecessary. Spacer experiments indicate that the enhancement of Raman cross sections decays slowly for distances of the scatterer from the silver of up to hundreds of Angstroms.

1 Tsang, Kirtley and Bradley, Phys. Rev. Letters 43, 772 (1979)

NC 13 Comparison of SERS Spectra and Voltammograms for CN^- Adsorbed on Ag and Cu Electrodes.* R.E. BENNER,† K.U. VON RABEN, R.K. CHANG, Yale U., and B.L. LAUBE, United Technologies Research Center—Using an optical multichannel analyzer, surface enhanced Raman spectra (SERS) from CN^- complexes adsorbed on Cu and Ag working electrodes have been detected at a rate of approximately one/sec during an oxidation/reduction cycle recorded by cyclic voltammetry. With 514.5 nm excitation, SERS from the Ag electrode is intense and reveals a dissolution and diffusion rate dependent sequence of peaks corresponding to AgCN, $Ag(CN)_2^-$, and $Ag(CN)_3^=$, while that from Cu is extremely weak with a peak centered near $\Delta\nu$ = 2100 cm^{-1} just discernible above a potential dependent broad background. Indicating that dispersion in the dielectric constant of the working electrode is a key parameter, SERS from Cu with 600 nm excitation becomes comparable in intensity to that from Ag. Consistent with the measured voltammograms, a sequence of peaks from various Cu-CN^- complexes is observed. Comparison of the two sets of results supports a model for SERS based on electron-hole pair excitation in conjunction with the formation of an adsorbed temporary-negative molecular ion complex.

*Supported by ONR Contract No. N00014-76-C-0643.

†Present address: Sandia Laboratories, Livermore, CA.

NC 14 Enhancement of Infrared Absorption from Molecular Monolayers with Thin Metal Overlayers. A. Hartstein, J. R. Kirtley and J. C. Tsang, IBM - T. J. Watson Research Center— The infrared absorption due to molecular monolayers of organic acids (4-nitrobenzoic acid, benzoic acid, and 4-pyradine-COOH) has been measured using the frustrated total internal reflection technique. Enhancements of the absorption have been observed due to the number of multiple total internal reflections, the presence of metal overlayers (Ag and Au) less than 100 Å thick, and the angle of the incident radiation. A maximum enhancement of close to 10^4 over the absorption from a single transmission through a monolayer has been obtained due to a combination of all of the above effects. This enhancement does not appear to be either metal dependent or molecule specific.

NC 15 Broad-Band Surface Electromagnetic Wave Propagation on Metal Surfaces.* Z. SCHLESINGER, Y.J. CHABAL†, and A.J. SIEVERS.--We have studied the propagation of broad-band surface electromagnetic waves (SEW's) on Ag. SEW's in the frequency range 500 cm^{-1} to 2500 cm^{-1} (60 to 300 meV) have been transmitted across a 1.2 cm long evaporated Ag film. The SEW's were excited by infrared radiation from an incoherent (Nernst Glower) source. An edge coupler[1], incorporated into a new geometry which permits the simultaneous excitation of SEW's over a broad band of frequencies, was used to launch and recover the surface waves. The respective frequency dependencies of the coupling angle and the refractive angle at which the beam enters and leaves the coupler tend to cancel in this dispersion compensating geometry. A signal to noise ratio of 30 to 1 in a 1 Hz bandwidth has been obtained.

*This work supported by AFOSR.

†Present address: Bell Telephone Labs, Murray Hill, NJ

(1) Y.J. Chabal and A.J. Sievers, Appl. Phys. Letters 32, 90 (1978).

NC 16 Infrared study of the W(100):H(1x1) system by Surface Electromagnetic Wave Spectroscopy*, Y.J. CHABAL+ and A.J. SIEVERS, Cornell U. --We report the first high resolution infrared observation of the ν_1 vibrational mode of hydrogen chemisorbed on W(100) at saturation coverage. A surface electromagnetic wave (SEW) coupling configuration has been developed which is UHV compatible. We find an order of magnitude increase in surface sensitivity over that obtained from reflection spectroscopy. At room temperature the center frequency of the observed ν_1 band is in good agreement with the frequency reported by electron Energy Loss Spectroscopy (ELS)[1] but the SEW line width is almost an order of magnitude smaller than the resolved line reported by ELS[1,4] . The apparent contradiction is resolved by invoking strong coupling between the ν_1 mode and the W surface phonons. The high resolution SEW technique measures the zero surface phonon ν_1 line but the low resolution ELS technique cannot separate the zero phonon line from the one phonon sidebands and measures both contributions.

*Supported by the Cornell Materials Science Center

+Present address: Bell Telephone Labs, Murray Hill

(1) A. Adnot and J.D. Carette, Phys. Rev. Lett. 39, 209 (77).

SESSION ND: SYMPOSIUM OF THE DIVISION OF ELECTRON AND ATOMIC PHYSICS: CHEMICAL EFFECTS IN ION-ATOM COLLISIONS

Friday afternoon, 28 March 1980; Sutton Ballroom Center at 2:00 P.M.; S. Shafroth, presiding

ND 1 Stereochemical Structures of Molecular Ions Determined Through "Coulomb Explosion" Techniques with Fast (MeV) Molecular-Ion Beams.* D.S. GEMMELL, *Argonne National Laboratory, Argonne, Illinois.* (30 min.)

High-resolution studies of the energy and angle distributions for fragments arising from the

Basic Optical Properties of Materials Summaries of Papers

Presented at the Topical Conference
on Basic Optical Properties of Materials
Held at the National Bureau of Standards
Gaithersburg, Maryland, May 5-7, 1980

Edited by:

Albert Feldman

Center for Materials Science
National Measurement Laboratory
National Bureau of Standards
Washington, D.C. 20234

In cooperation with:

The Optical Society of America
1816 Jefferson Place, NW
Washington, DC 20036

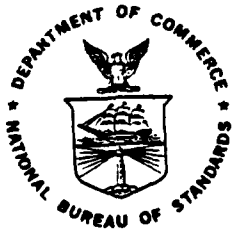

U.S. DEPARTMENT OF COMMERCE, Philip M. Klutznick, Secretary

Luther H. Hodges, Jr., Deputy Secretary

Jordan J. Baruch, Assistant Secretary for Productivity, Technology, and Innovation

NATIONAL BUREAU OF STANDARDS, Ernest Ambler, Director

Issued May 1980

Library of Congress Catalog Card Number: 80-600038

National Bureau of Standards Special Publication 574
Nat. Bur. Stand. (U.S.), Spec. Publ. 574, 252 pages (May 1980)
CODEN: XNBSAV

U.S. GOVERNMENT PRINTING OFFICE
WASHINGTON: 1980

For sale by the Superintendent of Documents, U.S. Government Printing Office, Washington, D.C. 20402
Price $6.50
(Add 25 percent for other than U.S. mailing).

INTERFEROMETRIC WAVELENGTH MEASUREMENT OF INFRARED SURFACE WAVES

Z. Schlesinger and A. J. Sievers
Laboratory of Atomic and Solid State Physics
Ithaca, N. Y. 14853

We have developed an interferometric technique for accurately measuring the wavelength of surface electromagnetic waves (SEW's) on coated metal surfaces. A variable pathlength, two-beam interferometer is employed in which the beam separation and interference take place entirely on the coated surface. The SEW's comprise one arm of the interferometer and bulk waves traveling just above the surface the other. The observed interferograms are in good agreement with model predictions.

Consider the propagation of a SEW across a partially coated surface such that the coated region occupies an intermediate section of the SEW path. The interference phenomenon involves the inhomogeneous nature of the SEW in an essential way. The field amplitudes of a SEW decay exponentially with distance away from the surface. This distance is very sensitive to small changes in the SEW wavelength which, in turn, depends on the state of the surface. For example, at the free space wavelength λ_o = 10 microns, the SEW on a bare gold surface has a wavelength λ_s = 9.999 microns and extends 60 microns in the air above the surface, while the SEW on a gold surface with a 0.05 micron Ge overlayer has a wavelength λ_s = 9.992 microns and extends only 20 microns above the surface. This discrepancy in the SEW extent makes it impossible for the bound SEW to maintain its integrity when it traverses a boundary between coated and uncoated regions of surface. Specifically the electromagnetic boundary conditions require that the tangential E and H fields be continuous at the boundary between the coated and uncoated regions at all heights above the interface. When the SEW is incident at the first coating edge this condition can be satisfied only if bulk (unbound) radiation is produced in transmission in addition to the transmitted (bound) SEW. At the far edge of the overlayer the SEW and bulk wave packet both contribute to the transmission of a bare metal SEW; however, these two contributions will in general no longer be in phase. The total intensity of the resultant SEW is

$$I(\ell) = I_{SEW}(\ell) + I_B(\ell) + 2\sqrt{I_{SEW}(\ell) I_B(\ell)}\cos\left[\frac{2\pi}{\lambda_o}\left(\frac{\lambda_o}{\lambda_s} - 1\right)\ell\right] \qquad (1)$$

where $I_{SEW}(\ell)$ and $I_B(\ell)$ are the component intensities and ℓ is the length of the coated region across which the beam travels. From the third term in Equation (1), the spatial period of the interference is

$$\Delta\ell = \frac{\lambda_o}{\lambda_o/\lambda_s - 1} \quad .$$

Because $\lambda_o/\lambda_s - 1$ is small, large interference periods will be produced by relatively short wavelength radiation (e.g. $\Delta\ell \cong 3$ mm at $\lambda \cong 10\mu$).

To test these conclusions, evaporated Ag and Au films were deposited on KCl couplers.(1) Over part of these rectangularly shaped films thin Ge overlayers of a triangular shape were then deposited. Both the metal and Ge film evaporations were carried out at a pressure of 4×10^{-6} torr. The SEW was launched from a CO_2 laser beam at one edge of the metal film by means of the edge coupling technique.(1) The length, ℓ, of the overlayer region probed by the beam was continuously varied by translating the film assembly in the plane of the surface but perpendicular to the beam direction. The transmission was measured as a function of ℓ for fixed overlayer thicknesses, d, and CO_2 laser wavelength, λ_o.

Ge overlayers ranging in thickness from $0.1\mu \leq d \leq 0.7\mu$ were studied in this manner in the range $9.2\mu \leq \lambda_o \leq 10.8\mu$. In each case the observed transmission characteristics and interference period were in agreement with model predictions.

In conclusion the SEW interferometer provides a unique method for studying thin films on metal surfaces. Not only is the attenuation of the SEW obtained but also, of equal spectroscopic significance, the wavelength of the SEW is measured, an undetermined quantity in ordinary transmission measurements.

ACKNOWLEDGMENTS

The authors acknowledge valuable conversation with R. Warner and Y. Chabal.

Work supported by AFOSR under Grant #AFOSR-76-3684. Additional support was received from the National Science Foundation under Grant No. DMR-76-81083 A02 and technical report #4210, to the Cornell Materials Science Center.

REFERENCE

1. Y. Chabal and A. J. Sievers, Appl. Phys. Lett. 32, 90 (1978).

Surface Science 102 (1981) L29–L34
© North-Holland Publishing Company

SURFACE SCIENCE LETTERS

BROADBAND SURFACE ELECTROMAGNETIC WAVE SPECTROSCOPY

Z. SCHLESINGER and A.J. SIEVERS
Laboratory of Atomic and Solid State Physics and Materials Science Center, Cornell University, Ithaca, New York 14853, USA

Received 10 July 1980

Broadband generation and spectroscopic detection of infrared surface electromagnetic waves (SEW's) are reported from 600 to 1800 cm^{-1}. For $KReO_4$ coated metal samples a sharp absorption line near 1000 cm^{-1} is used to compare the SEW and surface reflection spectroscopy (SRS) techniques. The integrated optical density of the absorption line is an order of magnitude larger with SEW spectroscopy than with SRS.

In this letter the first study of the propagation of surface electromagnetic waves (SEW's) excited by an incoherent source is reported. An edge coupler [1] incorporated into a dispersion compensating geometry which permits the simultaneous excitation of SEW's over a broad band of infrared frequencies has been developed and used to launch and recover the SEW's. A model system with an absorption line at 930 cm^{-1} has been studied using both SEW transmission spectroscopy and surface reflection spectroscopy (SRS). The measured optical density is an order of magnitude larger with SEW spectroscopy than with SRS.

Infrared surface electromagnetic waves are bound TM modes that exist at metal surfaces [2]. They propagate along the surface with a phase velocity less than, but close to, the speed of light and have field amplitudes which are maximal at the surface and decay exponentially with distance away from it. On good conductors, infrared SEW's propagate for distances many times their wavelength and can be used to probe the optical properties of surfaces [3,4]. In previously reported work, SEW's excited at a single frequency or several discrete frequencies by coherent radiation from infrared lasers have been used to study bare metal surfaces [5–8], metal surfaces with thin overlayers [8–11] and molecules adsorbed on metal surfaces [10–12]. In the past spectroscopic studies with thermal sources have not been possible with the SEW transmission technique because of insufficient energy throughput.

The standard two prism coupling configuration for launching and recovering monochromatic SEW's [5–8,10] is shown in fig. 1a. Monochromatic radiation impinges on the bottom face of the first prism, producing an evanescent wave which

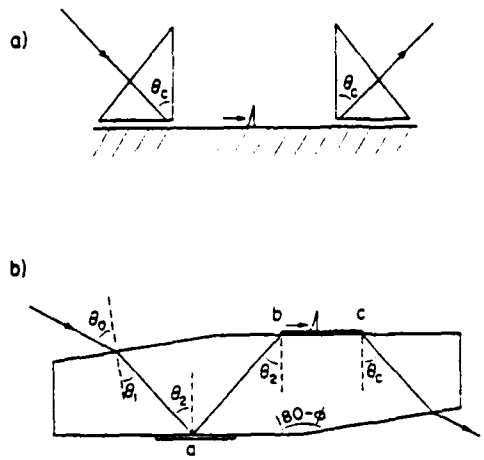

Fig. 1. Surface Electromagnetic Wave coupling schemes: (a) The two-prism evanescent wave coupling technique for launching and recovering monochromatic SEW's; (b) The edge coupling technique for launching and recovering polychromatic SEW's. The dispersive refraction of the incident beam partially compensates for the frequency dependence of the coupling angle. For KBr ($n \sim 1.50$) $\theta_c \sim 42°$, $\theta_0 = 56°$ and $\phi = 8°$.

excites SEW's on the metal surface. The coupling efficiency is virtually zero except at the critical angle, $\theta_c(\bar{\nu})$, defined as

$$\theta_c(\bar{\nu}) = \sin^{-1}[1/n(\bar{\nu})] , \tag{1}$$

where $\bar{\nu} = 1/\lambda$ and $n(\bar{\nu})$ is the frequency dependent index of refraction of the prism. Both the critical angle and the optimal gap spacing between the prism and the metal are frequency dependent. Thus, for a given alignment of the incident beam and the prism, coupling can be achieved only in a narrow band of frequencies.

The polychromatic coupling geometry used in our experiments is shown in fig. 1b. Transverse magnetic radiation (TM) polarized in the plane of fig. 1b, is incident on the coupler at a fixed angle, θ_0 (in the neighborhood of Brewster's angle). It enters the coupler at the frequency dependent angle,

$$\theta_1(\bar{\nu}) = \sin^{-1}[(\sin\theta_0)/n(\bar{\nu})] . \tag{2}$$

The beam is internally reflected by a metal film at point a and launches SEW's at the edge of a second metal film at point b [1]. The angle of incidence at the metal edge is

$$\theta_2(\bar{\nu}) = \phi + \sin^{-1}[(\sin\theta_0)/n(\bar{\nu})] , \tag{3}$$

where ϕ is the angle between the parallelepiped faces. A comparison of eqs. (3) and (1) shows that θ_2 and θ_c now depend similarly on frequency. If this edge coupler is aligned for optical coupling at a particular frequency, then it will also necessarily be

aligned for efficient coupling over a broad spectral region centered at that frequency.

To explore the sensitivity of the SEW technique, optically thick Au and Ag metal films were thermally evaporated onto KBr couplers at 1×10^{-7} Torr background pressure. Next, without breaking the vacuum, a $KReO_4$ overlayer was evaporated over part of each metal film. The polychromatic SEW measurement consisted of focussing a pencil of radiation (solid angle, approximately 4° in the air) from a Nernst glower source at the edge of the metal film to be studied (point b in fig. 1b). This beam, which was focussed with elliptical mirrors, excited SEW's which traversed the surface and reappeared at the far edge of the film as a collimated beam radiating into the coupler at the critical angle $\theta_c(\tilde{\nu})$. This beam was directed into a step-and-integrate Michelson interferometer and then focussed on an As : Si photoconductive detector.

The SEW transmission spectrum of a 1.7 cm long gold film covered by approximately one monolayer of $KReO_4$ is shown in fig. 2a. The $\tilde{\nu}_3$ mode of the ReO_4^- molecule [13] produces the absorption line at 930 cm^{-1}. Shown for reference in fig. 2b is the spectrum of the SEW transmission across a region of the same gold film with no $KReO_4$ overlayer. In each case, the instrumental resolution is 24 cm^{-1}. The spectral range is limited at the low frequency end by the beam splitter used in the interferometer and at the high frequency end by the increasing SEW attenuation.

The same sample has been studied by surface reflection spectroscopy using a two

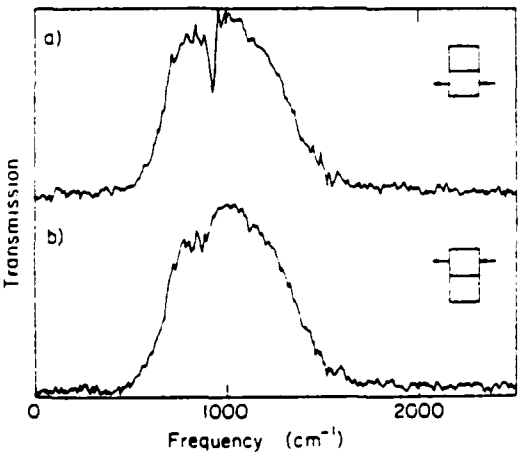

Fig. 2. Broadband Surface Electromagnetic Wave transmission spectra: (a) The transmission spectrum of SEW's traversing a 1.7 cm path across the surface of an optically thick gold film coated with an approximately 1 monolayer thick $KReO_4$ overlayer; (b) SEW transmission spectrum of an uncoated region of the same 1.7 cm gold film.

beam spectrometer with a variable angle reflectance accessory. Reflectance spectra have been taken with the spectrometer beam incident at angles ϕ, ranging from 55° to 70°. The presence of the $KReO_4$ overlayer produces a 25 cm^{-1} wide line at 932 cm^{-1} which is about 1% deep at $\phi = 60°$.

The effect of an overlayer on either the reflectance of or the SEW transmission across a metal can be calculated as an electromagnetic boundary value problem [4,14]. The overlayer is represented as a continuous medium of thickness d, separating infinite half spaces of metal and air. The properties of the overlayer are subsumed in a complex frequency dependent dielectric coefficient, $\tilde{\epsilon}_D$.

To first order, the effect of a thin overlayer on the metallic reflectivity of a TM polarized beam can be expressed as [14]

$$\frac{\Delta R}{R} = 8\pi\tilde{\nu}d(\cos\phi)\,\mathrm{Im}\left[\left(\frac{\tilde{\epsilon}_D - \tilde{\epsilon}_m}{1 - \tilde{\epsilon}_m}\right)\left(\frac{1 - (\tilde{\epsilon}_D\tilde{\epsilon}_m)^{-1}(\tilde{\epsilon}_D + \tilde{\epsilon}_m)\sin^2\phi}{1 - \tilde{\epsilon}_m^{-1}(1 + \tilde{\epsilon}_m)\sin^2\phi}\right)\right], \tag{4}$$

where $(\Delta R/R) = [R(0) - R(d)]/R(0)$ is the fractional change in reflectivity with $R(d)$ and $R(0)$ the respective reflectance spectra of the surface with and without the overlayer and $\tilde{\epsilon}_m$ = the frequency dependent dielectric function of the metal. In the infrared, $|\tilde{\epsilon}_D/\tilde{\epsilon}_m| \ll 1$, and at least up to $\phi = 85°$, $\cos^2\phi \ll |\tilde{\epsilon}_m|^{-1}$, hence eq. (4) simplifies to [15]

$$\frac{\Delta R}{R} = 8\pi\tilde{\nu}d\,\frac{\sin^2\phi}{\cos\phi}\,\mathrm{Im}\left(-\frac{1}{\tilde{\epsilon}_D}\right). \tag{5}$$

SEW transmission spectra can be calculated using the same model [4]. The full linear approximation theory cannot be used because even very thin overlayers can produce deep (≳50%) absorption lines. In the infrared to linear order in $\tilde{\nu}d$ one finds that

$$\ln\left(\frac{T(d)}{T(0)}\right) = 8\pi\tilde{\nu}d\left\{\pi l\tilde{\nu}\,\mathrm{Re}\left[\left(\frac{\tilde{\epsilon}_m}{\tilde{\epsilon}_m + 1} - \tilde{\epsilon}_m\right)^{1/2}\right]\right\}\mathrm{Im}\left(-\frac{1}{\tilde{\epsilon}_D}\right), \tag{6}$$

where $T(d)$ and $T(0)$ are the respective SEW transmission spectra with and without the overlayer and l is the length of the SEW path. When $\tilde{\epsilon}_m$ is represented by a Drude model, then in the relaxation limit eq. (6) reduces to

$$\ln\left(\frac{T(d)}{T(0)}\right) = 8\pi\tilde{\nu}d\left(\frac{\pi l\tilde{\nu}^2}{\tilde{\nu}_p}\right)\mathrm{Im}\left(-\frac{1}{\tilde{\epsilon}_D}\right), \tag{7}$$

where $\tilde{\nu}_p$ is the plasma frequency of the metal. We have verified that eq. (7) provides a reasonable approximation to the numerical results obtained from the exact equations for $KReO_4$ on Au in the 1000 cm^{-1} region.

From eq. (7) the size of the effect produced by the overlayer increases with the SEW path length, l, however the power transmitted across the surface at each frequency has an exponential dependence on l. The signal-to-noise in the spectrum is maximized when l is equal to the SEW propagation length, L, which is defined as the distance over which the intensity of a propagating SEW is attenuated by a fac-

tor of e^{-1}. For our evaporated gold films, L is in the neighborhood of 2 cm at 1000 cm^{-1}.

The optical density of the $KReO_4$ overlayer as probed by the SEW's is

$$D_{SEW} \equiv D(d) - D(0) = 0.43 \ln[T(0)/T(d)] , \tag{8}$$

where $D(d)$ is the optical density of the metal plus overlayer and $D(0)$ is the optical density of the bare metal. For the reflectivity measurement, the optical density of the overlayer is

$$D_{SRS} = 0.43 \ln[R(0)/R(d)] \simeq 0.43(\Delta R/R) . \tag{9}$$

The two techniques can be compared by integrating the measured optical density over the absorption line giving $\int D$. For the SEW absorption line shown in fig. 2a,

$$\int D_{SEW} = 6.9 \text{ cm}^{-1} \text{ (measured)} .$$

The integrated optical density of the line in the TM reflectance spectrum of the same film is

$$\int D_{SRS}\Big|_{\phi=60^\circ} = 1.3 \times 10^{-1} \text{ cm}^{-1} \text{ (measured)} .$$

By means of eq. (5), we can extrapolate this observed reflectivity result to the most sensitive experimentally feasible angle [16], $\phi = 80\text{–}85^\circ$, so

$$\int D_{SRS}\Big|_{\phi=83^\circ} = 7.0 \times 10^{-1} \text{ cm}^{-1} \text{ (extrapolated)} .$$

Hence the experimental ratio of the integrated optical densities of the absorption line in the SEW spectrum to that for a single bounce SRS measurement is $\geqslant 10$. This result should be compared with the ratio of the calculated integrated optical densities (eqs. (7) and (5)) which is

$$\frac{\int D_{SEW}}{\int D_{SRS}} = \frac{\pi l \tilde{\nu}_0^2/\tilde{\nu}_p}{\sin^2\phi/\cos\phi} . \tag{10}$$

For the parameters appropriate to the $KReO_4$: Au system, namely, $l = 1.7$ cm, $\tilde{\nu}_0 = 10^3$ cm^{-1} and $\tilde{\nu}_p = 72700$ cm^{-1} then

$$\frac{\int D_{SEW}}{\int D_{SRS}}\Big|_{\phi=83^\circ} = 9.1 \text{ (calculated)} .$$

which is in reasonable agreement with the experimental ratio obtained above.

With the dispersion compensated broadband SEW coupler we have demonstrated that an incoherent source can be used to excite SEW's over a broad band of IR frequencies. As long as the sample length is adjusted to be approximately equal to the SEW propagation length in the infrared region of interest, then SEW spectroscopy enhances the integrated optical density of an absorption feature by at least an order or magnitude over SRS. With a KRS-5 coupler it should be possible to use the broad band SEW spectroscopic technique described here down to a frequency of 250 cm^{-1}.

The authors wish to acknowledge valuable conversations with Y.J. Chabal, W.E. Moerner, and F.E. Pinkerton. This work was supported by AFOSR under Grant No. AFOSR-76-3684 and by the National Science Foundation through Grant No. DMR-76-81083A02 to the Cornell Materials Science Center. MSC Report No. 4271.

References

[1] Y.J. Chabal and A.J. Sievers, Appl. Phys. Letters 32 (1978) 90.
[2] A. Otto, Z. Physik 216 (1968) 398.
[3] V.M. Agronovich, Soviet Phys. Usp. 18 (1975) 99.
[4] R.J. Bell, R.W. Alexander, C.A. Ward and I.L. Tyler, Surface Sci. 48 (1975) 253.
[5] J. Schownwald, E. Burstein and J.M. Elson, Solid State Commun. 12 (1973) 185.
[6] J.D. McMullen, Solid State Commun. 17 (1975) 331.
[7] D.L. Begley, D.A. Bryan, R.W. Alexander, R.J. Bell and C.A. Goben, Surface Sci. 60 (1976) 99.
[8] D.A. Bryan, D.L. Begley, K. Bhasin, R.W. Alexander, R.J. Bell and R. Gerson, Surface Sci. 57 (1976) 53.
[9] Z. Schlesinger and A.J. Sievers, Appl. Phys. Letters 36 (1980) 409.
[10] K. Bhasin, D. Bryan, R.W. Alexander and R.J. Bell, J. Chem. Phys. 64 (1976) 5019.
[11] Y.J. Chabal and A.J. Sievers, J. Vacuum Sci. Technol. 15 (1978) 638.
[12] Y.J. Chabal and A.J. Sievers, Phys. Rev. Letters 44 (1980) 944.
[13] K. Nakamoto, Infrared and Raman Spectra of Inorganic and Coordinated Compounds (Wiley–Interscience, New York, 1978) p. 142.
[14] J.D.E. McIntyre and D.E. Aspnes, Surface Sci. 24 (1971) 417.
[15] H. Ibach, Surface Sci. 66 (1977) 56.
[16] R.G. Greenler, J. Vacuum Sci. Technol. 12 (1975) 1410.

Journal of Magnetism and Magnetic Materials 11 (1979) 109–112

INTRABAND MAGNETO-OPTICAL STUDIES OF InSb–NiSb EUTECTIC

A.K. CHIN * and A.J. SIEVERS
Cornell University, Ithaca, NY, USA

Received 15 August 1978; in revised form 11 October 1978

We present a magneto-optical study of the light hole valence band of InSb–NiSb eutectic. Far infrared transmission spectra are measured as a function of sample orientation, temperature (4.2–86 K), and magnetic field (0–80 kG). Acceptor energy levels and Luttinger coefficients are derived from the data.

1. Introduction

InSb–NiSb eutectic is a two phase material consisting of parallel aligned NiSb fibers within a semiconducting InSb matrix. Qualitatively, the combination of the two materials in this form results in a medium with highly anisotropic electrical properties [1]. The electrical conductivity is large in the direction of the metallic NiSb fibers and relatively small in the orthogonal direction. Also, due to the NiSb fibers, this eutectic displays magneto-resistive properties even more dramatic than those of pure InSb. At room temperature, a factor of 20 increase in resistance at 10 kG has been observed in InSb–NiSb [2]. These electrical properties have already resulted in a number of practical devices [1–3].

In this paper, we report on our magneto-optical determination of some of the InSb–NiSb energy band parameters. We present far infrared spectra of InSb–NiSb eutectic where the sample temperature is varied from 4.2–86 K and the magnetic field is varied from zero to 80 kG. The source of the eutectic spectra appears to be the InSb matrix modified by the NiSb fibers.

* Present address: Bell Laboratories, Murray Hill, NJ 07974, USA.

2. Experimental

2.1. Sample

The two phase InSb–NiSb eutectic is prepared by uniaxial solidification of the alloy consisting of 1.8 wt% NiSb [1]. The NiSb phase appears as single crystal rods with their long axis aligned parallel to the direction of solidification. These rods are spaced uniformly but randomly in the plane orthogonal to the growth direction (transverse plane). The rod dimensions and average separation are determined by the growth conditions. In the present samples, the NiSb fibers are 1 μm in diameter, 50 to 100 μm in length, and spaced approximately 3 μm apart in the transverse plane [4]. The InSb–NiSb samples are 8 mm diameter discs approximately 300 μm thick.

2.2. Magneto-optical results

The application of a magnetic field to the InSb–NiSb eutectic produces resonances that are both field and temperature dependent. Due to the number of transitions and the change in background transmission with magnetic field, the resonances are most easily studied by rationing the transmission at a field H to the zero field transmission. Fig. 1 shows some of this data at 4.2 K. The applied magnetic fields are indicated on the figure. The InSb–NiSb sample is oriented in the Faraday geometry with the long axis of the NiSb fibers

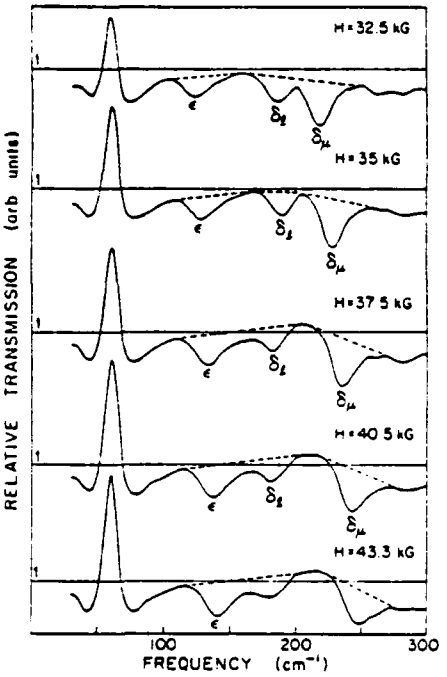

Fig. 1. Transmission of InSb–NiSb sample at the magnetic fields indicated relative to the zero field transmission. The three field dependent resonances are labeled δ_l, δ_μ, and ϵ.

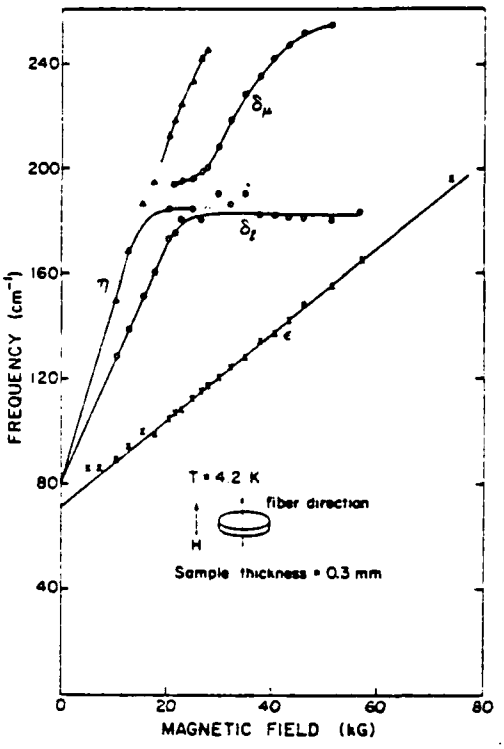

Fig. 2. Field dependence of transitions η, δ, and ϵ at 4.2 K. The data are obtained from a sample with the NiSb fibers parallel to the field.

parallel to H. The dashed lines are drawn to emphasize the field dependent resonances (δ_l, δ_μ and ϵ). These resonances are shown below to be independent of the orientation of the fibers with respect to H. The feature at 60 cm^{-1} is an anisotropic absorption line assumed to be a result of the NiSb fibers. Samples with the NiSb fibers orthogonal to the field direction do not show this.

Fig. 2 shows more clearly the field dependence of the center frequencies of resonances η, δ, and ϵ at 4.2 K. Data from eutectic samples with the NiSb fibers oriented parallel or orthogonal to H differed slightly; fig. 2 shows typical data from a sample with the NiSb fibers parallel to H. In the spectral region above 170 cm^{-1}, η and δ deviate from a linear field dependence. δ is pinned at the InSb LO phonon frequency of 190 cm^{-1}: the branch above 190 cm^{-1} is labeled δ_u and the pinned branch is labeled δ_l. The effective masses along with the zero frequency intercepts of η, δ, and ϵ are listed in table 1.

As the sample temperature is raised, the absorption strength of η, δ, and ϵ weaken and two new transitions (α and β) appear. At 86 K, only α and β are apparent in the transmission spectrum. Fig. 3 shows the field dependence of α and β. The data points are marked with (X) or (○) depending on whether the NiSb fibers are oriented orthogonal or parallel to H. The solid curves in fig. 3 are drawn through the combined set of data points and represent the field region over which

Table 1
Transition parameters

Transition	$m_{eff}/m_{electron}$	$\omega(H = 0$ kG) (cm^{-1})
α	0.0175	0
β	0.0655	26
η	0.0137	79
δ	0.0206	79
ϵ	0.0578	73

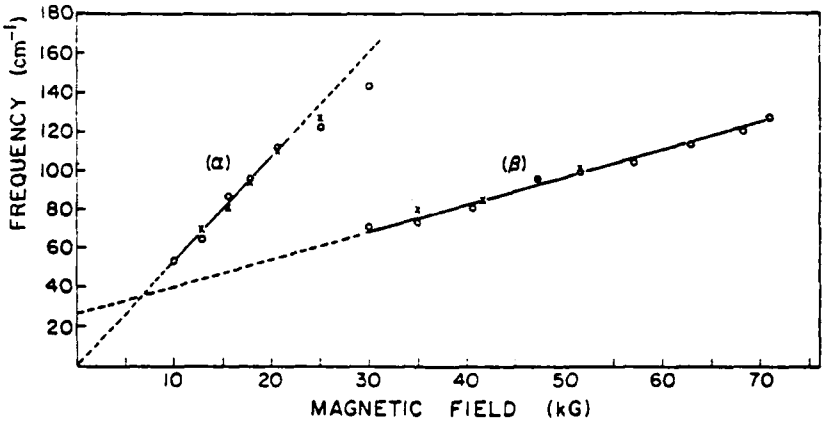

Fig. 3. Field dependence of transitions α and β at 86 K. The (×) and (○) points are data from samples with the NiSb fibers oriented orthogonal or parallel respectively to the field.

data were obtained. The dashed lines extrapolate the data to lower fields to indicate the zero field intercepts. The solid curve for α is extended beyond 20 kG to emphasize the deviation of the data from linearity. Table 1 lists the effective mass and zero field intercept of α and β.

3. Interpretation of results

The transitions observed in the transmission spectrum of InSb–NiSb are indicated by the arrows on the energy level diagram of fig. 4. For the most part, the energy scheme is similar but not identical to that of p-type InSb; the analysis used for InSb is applied to InSb–NiSb eutectic. Details of this analysis is found in ref. [5] and will be given in a following publication.

Three different types of energy levels are shown in fig. 4. A_0 and A_1 are the s-like ground and p-like first excited acceptor states respectively. The energy separation from the valence band of A_0 and A_1 may be obtained from the zero field intercepts of the transitions. Following the notation of refs. [6] and [7], $E_N^{\pm}(a, b)$ are the Landau levels of the light hole valence band. N is the orbital quantum number while (a) and (b) refer to the spin state. Assuming a spherically symmetric valence band, $E_N^{\pm}(a, b)$ are a function of the three Luttinger coefficients [8] γ_1^L, and $\bar{\gamma}^L$, and κ^L. This assumption should be valid for InSb–NiSb since the data is sample orientation independent. The Luttinger coefficients are determined by the effective masses of the resonances. Finally, $(NM\lambda)a, b$ are the impurity states associated with $E_N^{\pm}(a, b)$. The notation of ref. [9] is used. M is the component of the angular momentum along H. λ is the number of modes in the impurity wave function along H. The values of $(NM\lambda)a, b$

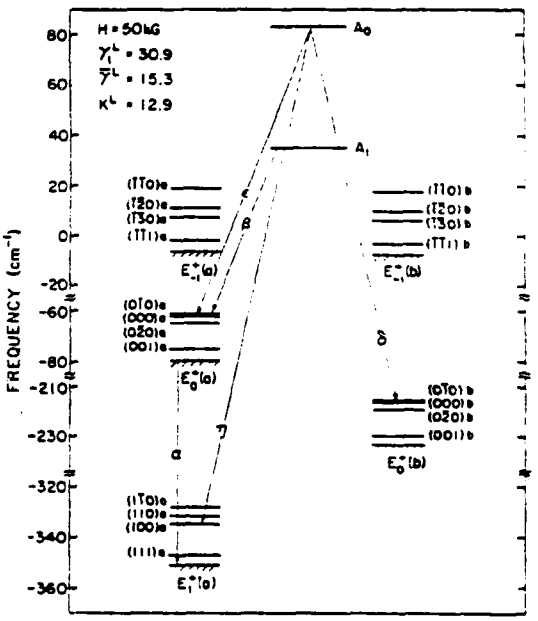

Fig. 4. Energy level diagram for InSb–NiSb showing the observed transitions.

calculated for InSb are used to analyze the eutectic data [9].

As shown in fig. 4, α is a light hole cyclotron resonance. The deviation from a linear field dependence is probably due to free hole–phonon interaction in analogy to the coupling of the electron cyclotron resonance with the LO phonon [10]. Nonparabolicity is not considered to be the cause of the nonlinear field dependence of α since the light hole valence band of the eutectic has been determined to be highly parabolic from a high (300 kG) magnetic field study [5]. Free hole–phonon interaction has not been observed in p-type InSb. η, δ, and ϵ all initiate from the ground acceptor state A_0; the final states are assumed to be the p-like impurity levels (100)a, (000)b, and (000)a respectively. The nonlinearity in the field dependence of η and δ is due to bound hole–phonon interaction [11]. β is a transition from the first excited acceptor level A_1 to the s-like impurity level (010)a. The difference in the effective masses of β and ϵ is attributed to the field dependence of A_0 in similarity to the central cell shift of the donor ground state in InSb [12].

Analysis of the InSb–NiSb data in table 1 gives the following results. The Luttinger coefficients for the valence band are $\gamma_1^L = 30.9$, $\bar{\gamma}^L = 15.3$, and $\kappa^L = 12.9$. A_0 and A_1 are 83 cm^{-1} and 26 cm^{-1} respectively from the zero field valence band edge. These values are similar to those of p-type InSb.

Acknowledgements

This work has been supported in part by AFOSR under contract No. AFOSR-78-3684. Additional support was received from the National Science Foundation under grant DMR-76-81083 through the Cornell Materials Science Center Technical Report #3067.

References

[1] F.S. Galasso, J. Metals 19 (1967) 17.
[2] H. Weiss and M. Wilhelm, Z. Phys. 176 (1963) 399.
[3] B. Paul and H. Weiss, Solid State Electronics 11 (1968) 979.
[4] Samples provided by Siemens Research Laboratories, Erlangen, Germany.
[5] A.K. Chin, Ph.D. Thesis, Cornell University (1977).
[6] C.R. Pidgeon and R.N. Brown, Phys. Rev. 146 (1966) 575.
[7] C.R. Pidgeon and S.H. Groves, Phys. Rev. 186 (1969) 824.
[8] J.M. Luttinger, Phys. Rev. 102 (1956) 1030.
[9] P.J. Lin-Chung and B.W. Henvis, Phys. Rev. B12 (1975) 630.
[10] C.J. Summers, K.B. Dennis, B.S. Wherrett, P.G. Harper and S.D. Smith, Phys. Rev. 170 (1967) 755.
[11] R. Kaplan, K.L. Ngai, B.W. Henvis, Phys. Rev. Lett. 28 (1972) 1044.
[12] R. Kaplan, Phys. Rev. 181 (1969) 1154.

Solid State Communications, Vol. 35, pp. 991–993.
Pergamon Press Ltd. 1980. Printed in Great Britain.

ORIGINS OF VERY SHALLOW PHOTOCONDUCTION IN Ge:Sb*

E.A. Schiff†

Laboratory of Atomic and Solid State Physics and Materials Science Center, Cornell University, Ithaca, NY 14853, U.S.A.

(*Received* 20 *March* 1980 *by J. Tauc*)

Three new effects in the very shallow photoconduction spectrum ($\hbar\omega <$ 5 meV, $T \sim 0.4$ K) of Ge:Sb have been observed: the spectrum is found to depend strongly on electric-field, background excitation spectrum, and on the spectrometer chopping frequency. These effects are interpreted as evidence that the spectra are the consequence of two distinct trapping centers whose spectra overlap; they thus do not support the interpretation of this photoconduction as due entirely to a D^- band.

AT VERY LOW TEMPERATURES ($T < 1.2$ K) lightly doped, uncompensated Ge:Sb exhibits photoconduction at optical energies substantially less than the threshold energy for ionization of a neutral, isolated Sb donor (10 meV) [1, 2]. Analogous very shallow photoconduction is also observed for other dopants in both Ge and Si [3, 4]. This photoconduction is due to the photodetachment of electrons from very shallowly bound traps which are populated by exposure of the sample to weak extrinsic background radiation. The impurity center binding this electron has previously been identified as the D^- center formed by the capture of a photocarrier by a neutral donor and in analogy with the atomic H^- ion.

One of the most perplexing aspects of the spectra observed in this manner has been their variability. The observed spectrum is markedly dependent in both shape and magnitude on temperature, the dopant and its doping level, uniaxial stress, and magnetic field. Of these spectral changes the most central to understanding the origins of very shallow photoconduction is the temperature dependence of the spectrum; several authors [2, 3, 5] have reported that the spectrum's threshold shifts to higher energy as the temperature is increased. These shifts have been attributed either to the formation of impurity bands from a single type of defect (cf. the D^-) [2, 3] or to the presence in the spectrum of components originating from additional shallow levels ($D^- - D^*$, D_2^-, etc.) [5].

Here I shall report several new experiments on very shallow photoconduction in Ge:Sb which show spectral shifts closely related to the shifts seen when the specimen temperature is varied. The most important of these results is the observation that the bias electric-field used to measure the photoconductivity spectrum modifies the spectral shape. A simple method for decomposing the spectrum into two different but field-independent spectra has been found. The changes in the spectral shape seen with electric field, temperature, spectrometer chopping frequency and background excitation spectrum can be accounted for by changing the weighting, but not the shape, of these two components of the observed spectrum. These new observations thus strongly support the existence of two distinct types of shallow center in Ge:Sb.

The photoconduction spectra reported here were measured using lamellar and Michelson Fourier transform spectrometers. The specimen temperature ranged from 0.4 to 4.2 K. Eight specimens of Ge:Sb were examined; only two of these specimens exhibited measurable shallow trap photoconduction. The failure of most specimens to exhibit very shallow photoconduction is usually attributed to fairly high compensation ratios ($N_A/N_D > 0.05$) [1], although the importance of low compensation is not quantitatively understood. All of the spectra reported here are from the purest specimen ($N_D = 3.3 \times 10^{14}\,\mathrm{cm}^{-3}$, $N_A = 4.4 \times 10^{12}\,\mathrm{cm}^{-3}$). The effects reported here were also observed in another Ge:Sb specimen and in a Ge:Ga specimen.

All of the photoconduction spectra were taken in the presence of significant cold-filtered room-temperature background radiation. This radiation generates a background photoconductivity by ionizing neutral Sb donors; the background photoconductivity was always much larger than the specimen's dark conductivity. Both the phase and magnitude of the shallow trap photoconduction were recorded as a function of the spectrometer chopping frequency; these measurements are equivalent to time-domain measurements of the spectrum, albeit on the time scale of tens of milliseconds.

* Research supported by AFOSR (78-3684), USDOE (EY-76-S-01-3151), and by the Cornell Materials Science Center (NSF DMR76-81083).

† Present address: James Franck Insitute, University of Chicago, Chicago, Illinois 60637.

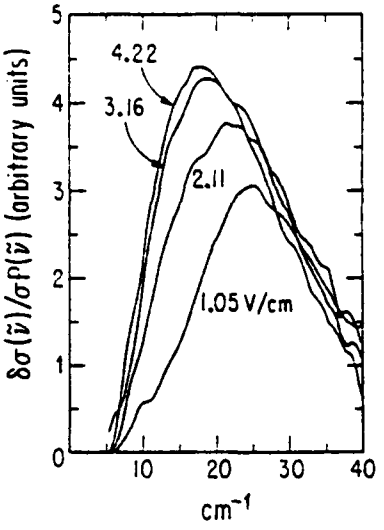

Fig. 1. Ratio of the relative photoconduction spectrum $\delta\sigma(\tilde{\nu})/\sigma$ to spectrometer power spectrum $P(\tilde{\nu})$ for four bias electric fields. σ: background photoconduction. 0.49 K, KI composte cold filter ($\tilde{\nu} < 100\,\mathrm{cm}^{-1}$).

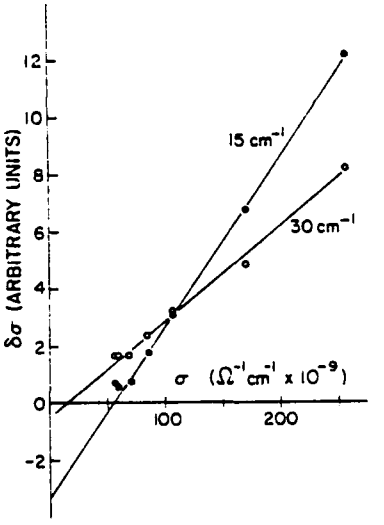

Fig. 2. Shallow trap photoconduction $\delta\sigma$ at 15 and 30 cm^{-1} as a function of the sample's electric field dependent background photoconductivity σ. $\delta\sigma$ at each wavenumber has been normalized by the intensity by the intensity of the spectrometer radiation determined by a 0.4 K bolometer. $\tilde{\nu} < 100\,\mathrm{cm}^{-1}$; $T = 0.43$ K.

The shallow photoconduction spectra observed at four electric field levels are plotted in Fig. 1; an increase in the field clearly enhances the strength of the spectrum in the low-frequency threshold region relative to the tail of the spectrum. The absolute normalization of these spectra is important: the intensity of the photoconduction spectrum, $\delta\sigma(\tilde{\nu}, E)$ has been divided by the field-dependent background photoconduction $\sigma(E)$ ($\tilde{\nu}$ is the optical frequency in wavenumber (cm^{-1}) units; E is the electric field). In addition the spectra are ratioed to the power spectrum of the spectrometer. The origin of the electric-field dependence of $\sigma(E)$ itself is a matter of mild controversy, and in fact no universal explanation, valid for any specimen, can be offered. However, additional experiments on the neutral donor photoconduction spectrum ($\tilde{\nu} > 70\,\mathrm{cm}^{-1}$) and its field dependence for th[illegible] specimen are consistent with the picture that the dependence $\sigma(E)$ is due to the apparent field-ionization [7] of excited states of the neutral Sb donor. The field-ionization of these states contributes both to an increase in the carrier generation rate (via field assisted ionization of donors photoexcited by the background radiation) and to an increase in the recombination lifetime (as a consequence of "cascade recombination", in which carriers recombine by falling through these same excited states). The optical cold filter for these data was chosen to emphasize the change in the generation rate, which accounts for nearly 50% of the observed variation of $\sigma(E)$; other choices of optical cold filters do influence the observed spectra.

If the variation $\sigma(E)$ were entirely due to changes in the generation rate, a simple proportionality between $\delta\sigma(\tilde{\nu}, E)$ and $\sigma(E)$ would be expected, according to the argument that the density of carriers in shallow levels is proportional to the density of carriers in the conduction band. This hypothesis has been tested in Fig. 2. The expected linear relationship is obtained, but the 15 cm^{-1} line has a substantial negative intercept. This negative intercept is the origin of the field-dependence of the spectra.

The $\delta\sigma$ vs σ relations obtained thus suggest the following model for very shallow photoconduction. The spectra consist of one component which scales with the background photoconduction, and an additional negative component which is field-independent:

$$\delta\sigma(\tilde{\nu}, E) = \alpha(\tilde{\nu})\sigma(E) + \beta(\tilde{\nu}).$$

The spectra obtained from this decomposition in the zero-field limit are presented in Fig. 3. The "photocarrier" spectrum is $\alpha(\tilde{\nu})$, and the "impurity conduction" spectrum is $\beta(\tilde{\nu})$. These labels refer to an hypothesis for the photoconductive mechanisms underlying these components, and in particular the negative component is speculatively attributed to a reduction in the impurity conduction of trapped carriers.

The validity of this decomposition, which originates with the electric-field dependence of the spectrum, is strongly supported by its success in describing the dynamics of the shallow photoconduction. In particular, the rather long trap lifetimes obtainable at very low temperatures give rise to a photoconduction signal in quadrature with the chopped spectrometer illumination.

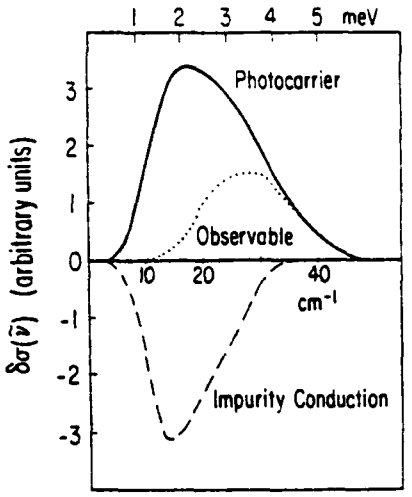

Fig. 3. Decomposition of the zero-field photoconduction spectrum into two components; experimental conditions are those of Fig. 2.

This quadrature spectrum is given quite precisely by the "photocarrier" component of Fig. 3 alone; the quadrature spectrum does not show the electric-field dependence of the spectrum measured in phase with the spectrometer illumination.

I associate the two components of the photoconduction spectrum with two distinct shallow centers, differing greatly in photoconduction mechanism and characteristic lifetimes, but with remarkably similar spectra and magnitudes of photoconductive response. Rate equation models for two centers which predict the two components' dependences on electric-field, chopping frequency, and the background excitation spectrum have been obtained and will be presented elsewhere. These models do not account for the similarity of the two centers' spectra or, as yet, for the comparable magnitudes of their respective photoconductivities. The convincing identification of these centers, and of their relationship to the ϵ_2 activation energy [8] of importance in the Mott description of the metal-insulator transition, are important avenues for further research.

Acknowledgements – I wish to thank P. Norton for suggesting these experiments, for his collaboration in their early stages, and for many illuminating discussions. I thank A.J. Sievers for his encouragement and advice. W.J. Moore kindly provided the Ge:Ga specimens.

REFERENCES

1. E.M. Gershenson, G.N. Gol'tsman & A.P. Mel'nikov, *JETP Lett.* 14, 185 (1971) [*Pis'ma Zh. Eksp. Teor. Fiz.* 14, 3 (1971)].
2. M. Taniguchi, M. Hirano & S. Narita, *Phys. Rev. Lett.* 35, 1095 (1975); M. Taniguchi & S. Narita, *J. Phys. Soc. Japan* 47, 1503 (1979).
3. P. Norton, *J. Appl. Phys.* 47, 308 (1975); P. Norton, *Phys. Rev. Lett.* 37, 164 (1976).
4. V.N. Aleksandrov, E.M. Gershenson, A.P. Mel'nikov & N.A. Serebryakova, *Sov. Phys. – JETP* 43, 305 (1976); [*Zh. Eksp. Teor. Fiz.* 70, 586 (1976)].
5. V.N. Aleksandrov, E.M. Gershenson, N.A. Serebryakova, A.P. Mel'nikov & R.M. Rabinovich, *JETP Lett.* 22, 282 (1975); [*Pis'ma Zh. Eksp. Teor. Fiz.* 22, 573 (1975)]; V.N. Aleksandrov, E.M. Gershenson, A.P. Mel'nikov, R.I. Rabinovich, N.A. Serebryakova, Yu.V. Tomach & V.A. Zayats *Physics of Semiconductors 1978* (Edited by B.L.H. Wilson), p. 977. Institute of Physics, Bristol (1979).
6. P.R. Bratt, *Semiconductors and Semimetals* 12 (Edited by R.K. Willardson and A.C. Beer), p. 116ff. Academic Press, New York (1977); E.E. Godik, Yu.A. Kuritsyn & V.P. Sinis, *Sov. Phys. Semicond.* 8, 1373 (1975) [*Fiz. Tekh. Poluprov.* 8, 2116 (1974)].
7. Field-assisted ionization is observed as an electric-field variation in the neutral donor photoconduction spectrum threshold. The physics of this effect has never been satisfactorily explained; see L.V. Berman, T.I. Domasheva & A.G. Zhukov, *Sov. Phys. Semicond.* 7, 1256 (1974) [*Fiz. Tekh. Poluprov.* 7, 1882 (1974)] and references therein.
8. H. Fritzsche, *J. Phys. Chem. Solids* 6, 69 (1958); E.A. Davis & W.D. Compton, *Phys. Rev.* 140, A2183 (1965).


DATE
ILME